Intérêt des invariants pour analyser l'anisotropie induite par l'endommagement dans les bétons

GDR-GDM La Rochelle

A. Fau

26.06.2024

Laboratoire de Mécanique Paris-Saclay

Collaboration with Ammar Basmaji, U. Nackenhorst, Leibniz Universität Hannover

R. Desmorat, Laboratoire de Mécanique Paris-Saclay

Introduction

Concrete at a mesoscopic scale with accurate representation of the mesostructure, volume fraction, shapes.

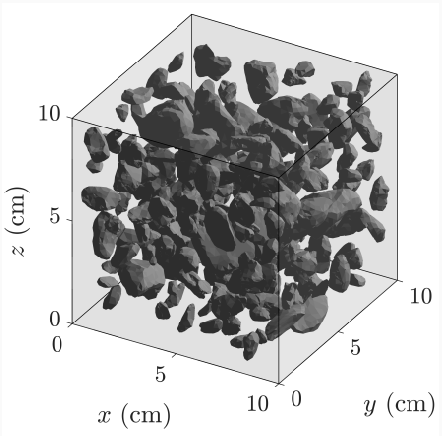

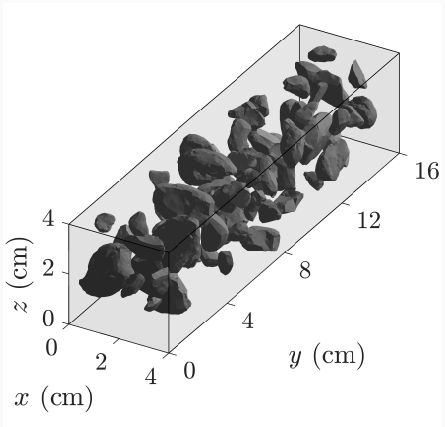

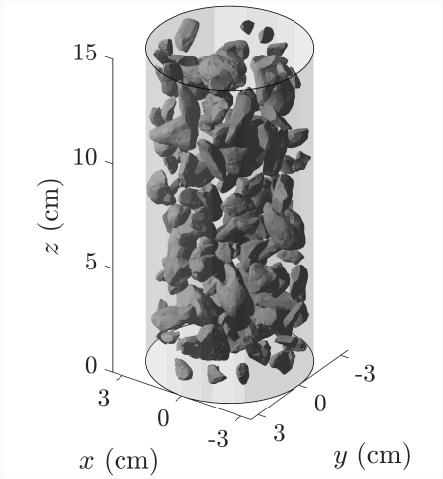

- Elastic aggregates with real shapes
- Damaging mortar
  - Representing properly the difference between tension and compression requires anisotropic damage
  - Dedicated model for representing cyclic/alternate loading cases

Generation of a virtual concrete specimen with aggregates of arbitrary shapes

Laser-scanned aggregate database

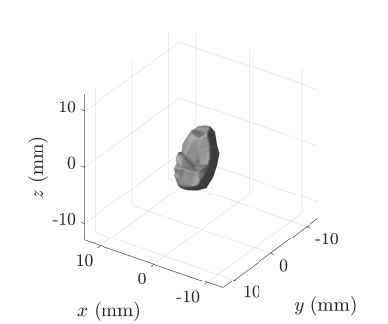

(a) $K = 394$ vertices.

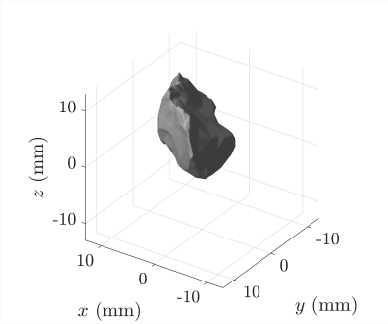

(b) $K = 783$ vertices.

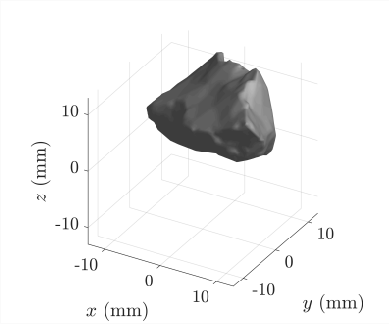

(c) $K = 811$ vertices.

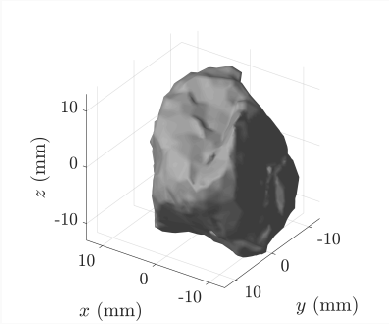

(d) $K = 1590$ vertices.

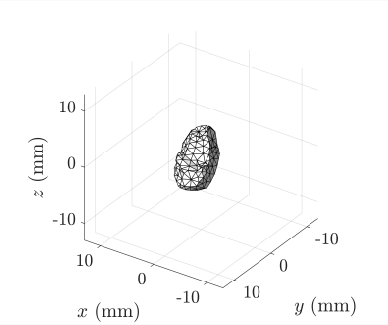

(e) $K = 141$ vertices.

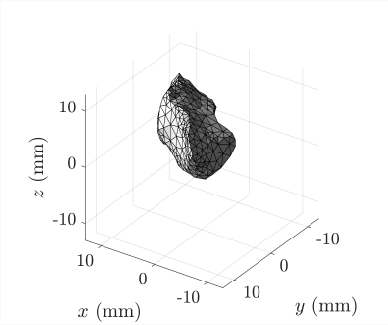

(f) $K = 322$ vertices.

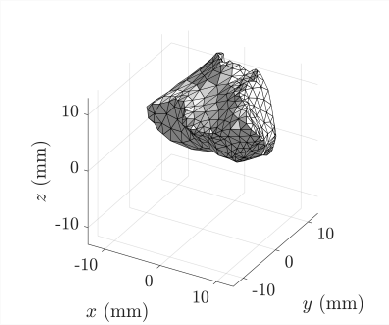

(g) $K = 561$ vertices.

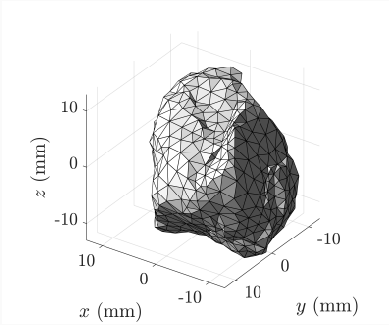

(h) $K = 691$ vertices.

Examples of real-shaped aggregates from the database (Thilakarathna 2020)(top) and their FE discretization (bottom).

Target Fuller's curve and computed granulometry curves

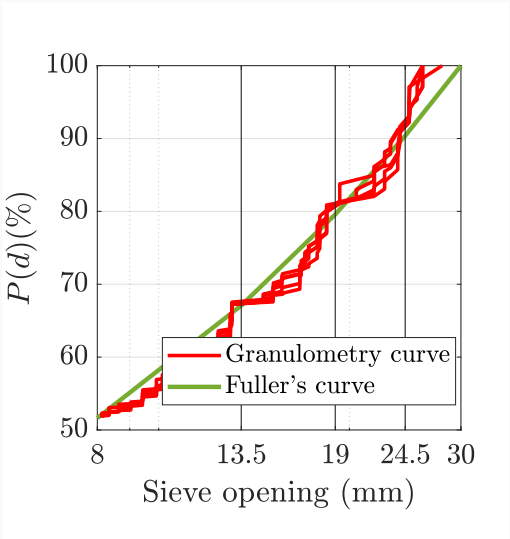

(a) Real-shaped

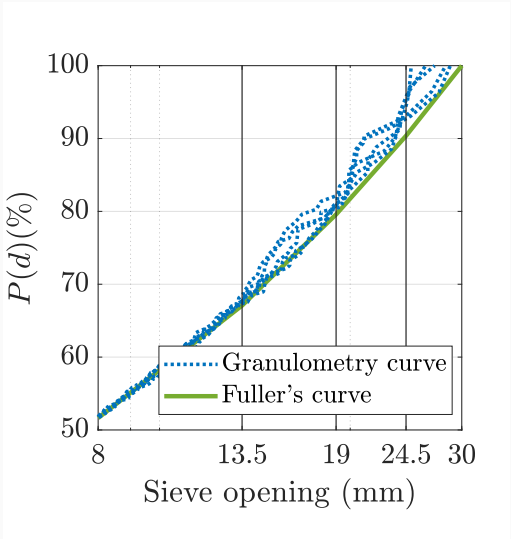

(b) Ellipsoidal

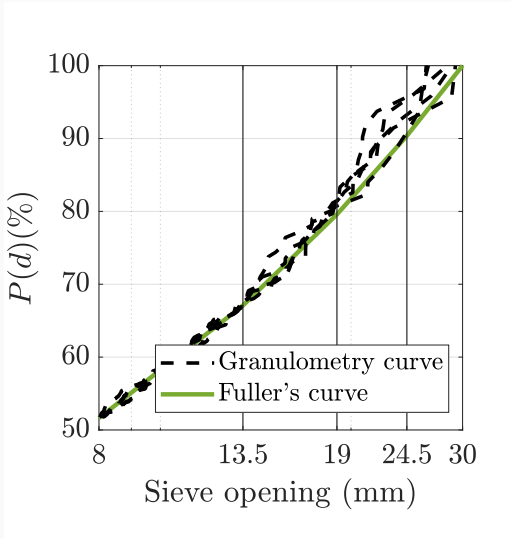

(c) Spherical

All designed specimens have an aggregate volume fraction ranging from 20.0% to 20.1%

Granulometric distribution optimised for optimal compacity (Fuller, 1907)

$$P(d) = 100\sqrt{\frac{d}{d_{\max}}},$$

where $d_{\max}$ is the maximum size of the aggregates.

Packing algorithm – Oriented Bounding Box method

The aggregates generated are used to fill a desired fraction of the virtual concrete volume using a packing algorithm that prevents aggregates from overlapping.

The Oriented Bounding Box method (Barequet and Har-Peled, 2001) uses the covariance matrices of the vertices to embed the aggregates in oriented rectangular cuboids.

It has been used

- in the context of virtual prototyping and mechanical assembly tests (Redon et al, 2002)
- in free-form surface machining (Ding et al, 2004),
- in medical physics (Lahanas et al, 2000),
- for the interference detection in video games (Van Verth and Bishop, 2015, Lazaridis, 2021).

Seems not to have been applied to the design of concrete mesostructures.

Oriented Bounding Boxes

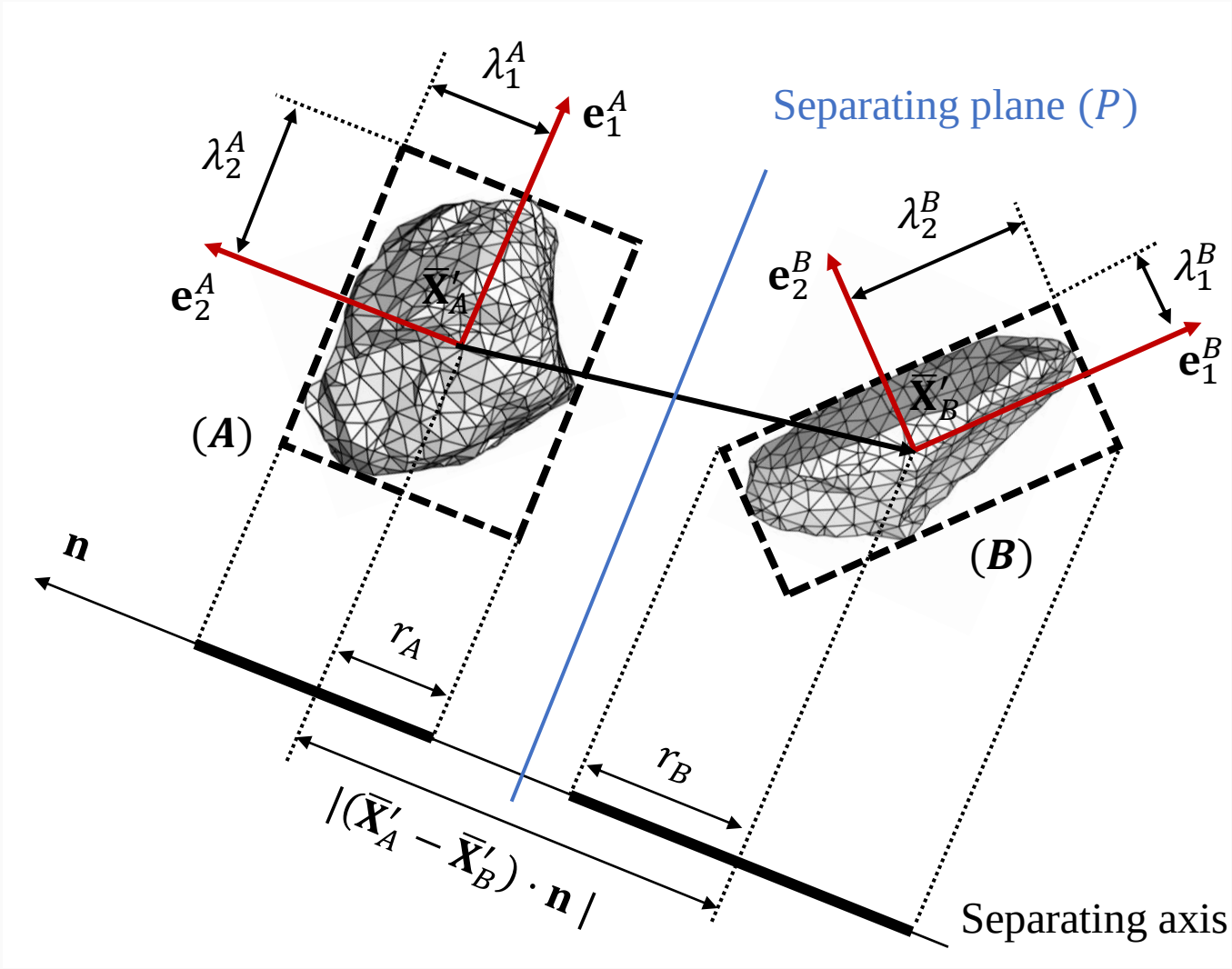

Two Oriented Bounding Boxes (A) and (B) separated by a separating plane.

Mesostructures with various aggregate volume fractions

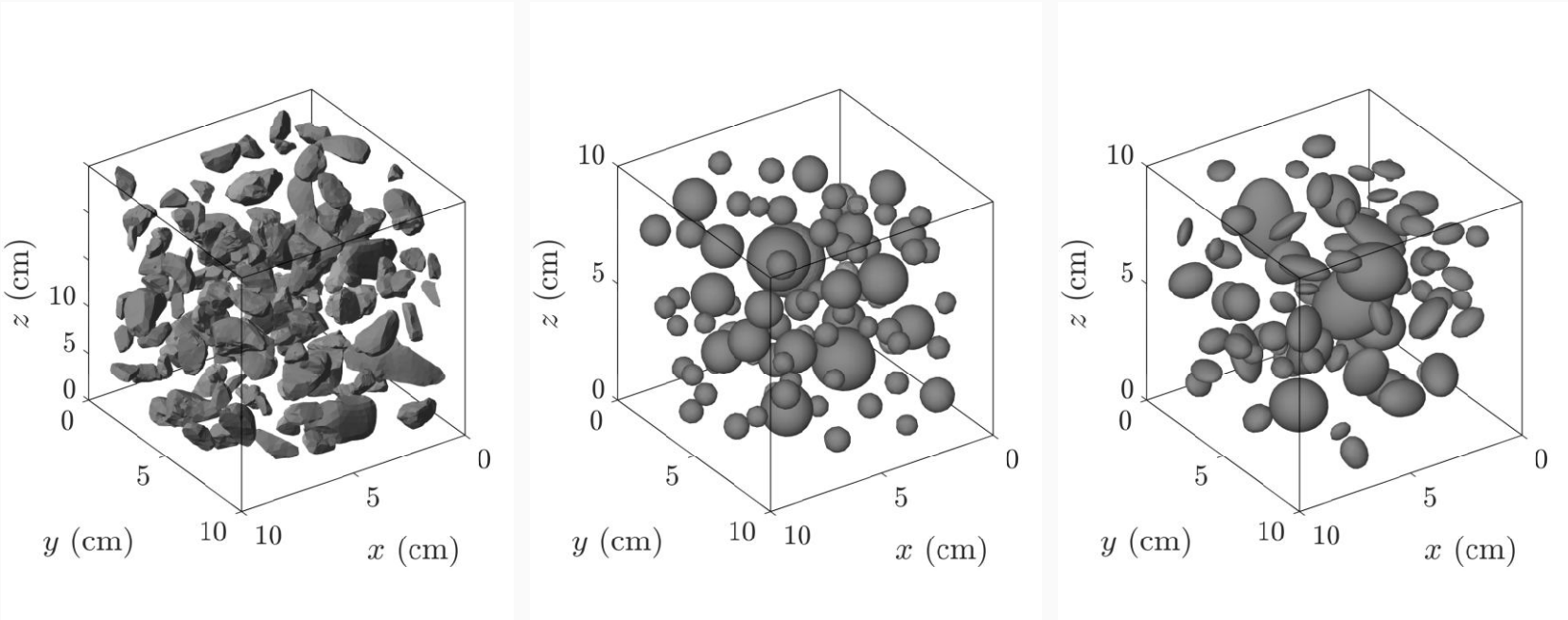

(a) Real-shaped aggregates **(b)** Spherical aggregates **(c)** Ellipsoidal aggregates

Examples of mesostructures of cubic concrete specimens with different shapes of randomly packed aggregates, for an aggregate volume fraction of 20%.

Wall effect reproduced

A virtual concrete specimen

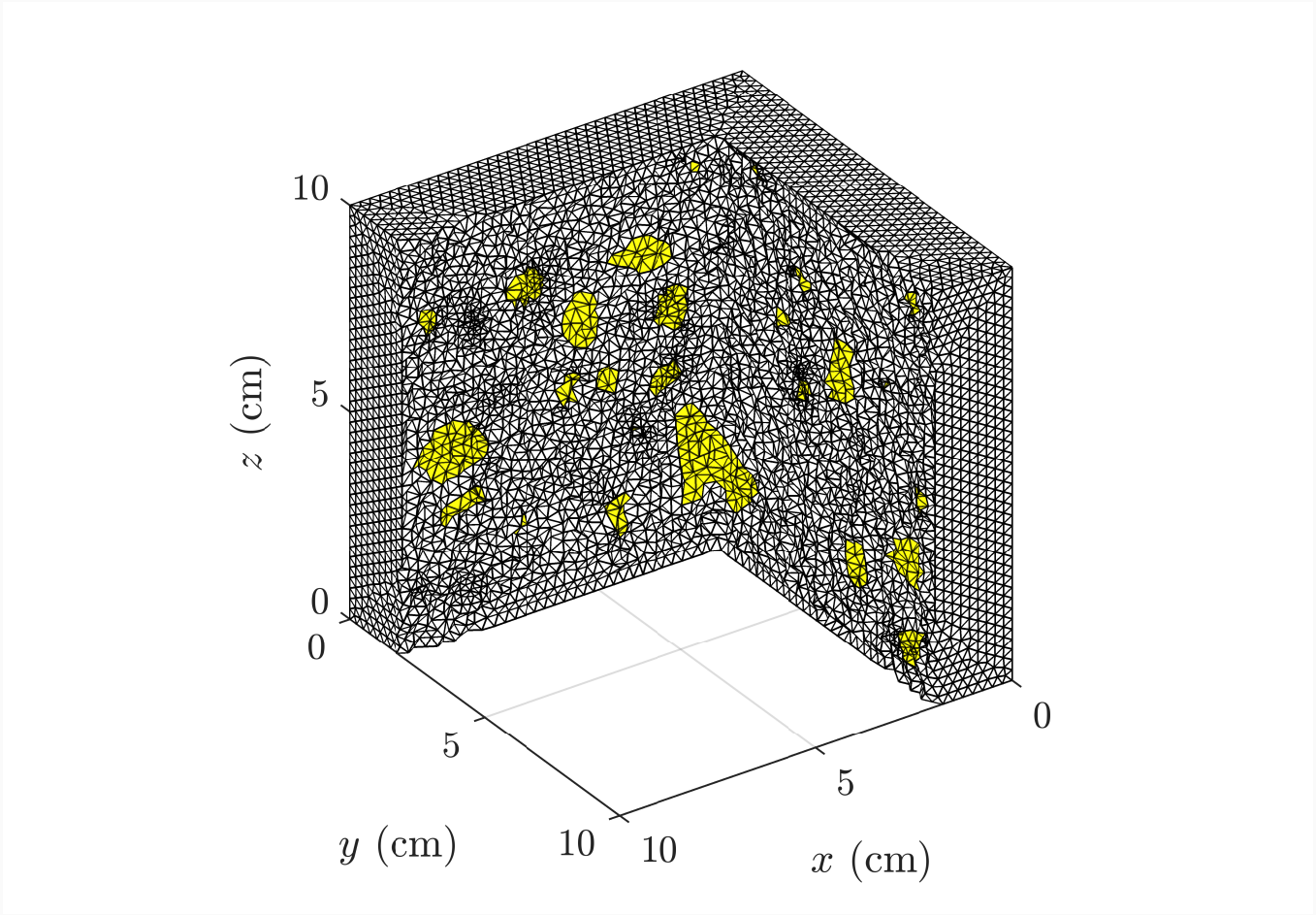

Section views of the FE mesh of a virtual concrete specimen (real-shaped aggregates in yellow)

Finite-element discretization

- linear tetrahedral elements,
- elements indexed according to their respective materials, aggregates and mortar,
- maximum element size $h_{max} = \ell_{int}/5 = 2$ mm equal to the fifth of the nonlocal internal length for mortar,
- approximately $700,000$ elements and $370,000$ degrees of freedom for the real-shaped aggregate specimens (minimum element size $h_{min} = 0.5$ mm),
- approximately $500,000$ elements and $275,000$ degrees of freedom for the spherical or ellipsoid aggregate specimens.

Nonlocal anisotropic damage model for mortar subjected to alternate/cyclic loading

Damage models for concrete subjected to cyclic loading

Alternate/cyclic response by local isotropic damage models:

- by pure 1D damage model (La Borderie, 1991)
- by internal sliding coupled with damage (Ragueneau et al, 2000, Richard and Ragueneau, 2013)
- by plastic-damage model (Grassl and Jirasek, 2006, 2008)

Concrete mesostruture computations

- One computation with **local** anisotropic damage model (Kim and Abu Al-Rub, 2011)
- Very few computations with **nonlocal/gradient/phase field** isotropic damage (Unger and Eckardt, 2011, Ren et al, 2024, Zhang et al, 2024)
- No computation with **nonlocal anisotropic** damage
- No computation for **cyclic loading**

Anisotropic damage model (for mortar)

Use Ladevèze (1983, 1995) 2nd order tensorial damage variable

$$\boldsymbol{H} = (\mathbf{1} - \boldsymbol{D})^{-\frac{1}{2}}$$

unbounded and such as $\boldsymbol{H} = \mathbf{1}$ when $\boldsymbol{D} = 0$

Extend to alternate/cyclic loading the model of (Desmorat, 2016)

- **Elasticity coupled with anisotropic damage**

$$\tilde{\boldsymbol{\sigma}} = \mathbb{E} : \boldsymbol{\varepsilon} = 2G\,\boldsymbol{\varepsilon}^D + K\,\mathrm{tr}\,\boldsymbol{\varepsilon}\,\mathbf{1}, \qquad (\cdot)^D = (\cdot) - \frac{1}{3}\,\mathrm{tr}(\cdot)\,\mathbf{1}$$

  where G shear modulus, K bulk modulus

- Symmetric **effective stress**, independent from Poisson's ratio,

$$\tilde{\boldsymbol{\sigma}} = \left(\boldsymbol{H}\cdot\boldsymbol{\sigma}^D\cdot\boldsymbol{H}\right)^D + \frac{1}{3}\left[\frac{1}{3}\,\mathrm{tr}\,\boldsymbol{H}^2\langle\mathrm{tr}\,\boldsymbol{\sigma}\rangle - \langle -\mathrm{tr}\,\boldsymbol{\sigma}\rangle\right]\,\mathbf{1}$$

  where $\langle x\rangle = \max(0, x)$ positive part of x

Anisotropic damage model for alternate/cyclic loading

- Lemaitre and Mazars (1980) **criterion function**

$$f = \varepsilon_{\text{Maz}} - \kappa \leq 0, \qquad \varepsilon_{\text{Maz}} = \sqrt{\langle \boldsymbol{\varepsilon} \rangle^{+} : \langle \boldsymbol{\varepsilon} \rangle^{+}}$$

  $\langle \cdot \rangle^{+}$: positive part of symmetric 2nd order tensor

- **Consolidation function** extended to alternate loading by the active damage concept (Souid et al 2009, Chambart et al, 2010))

$$\kappa = \kappa_0 + S R_v^s \left[(\boldsymbol{H} - \mathbf{1}) : \tilde{\boldsymbol{Q}} \right]^{1/a}, \quad \text{with} \quad \tilde{\boldsymbol{Q}} = \frac{\langle \tilde{\boldsymbol{\varepsilon}} \rangle^{+}}{\max_I \langle \tilde{\varepsilon}_I \rangle}, \quad \tilde{\boldsymbol{\varepsilon}} = \mathbb{E}^{-1} : \boldsymbol{\sigma}$$

  $R_v(\operatorname{tr} \boldsymbol{\sigma} / \sigma_{\text{vM}})$: triaxiality function (and $\sigma_{\text{vM}} = \sqrt{\frac{3}{2} \boldsymbol{\sigma}^D : \boldsymbol{\sigma}^D}$)

Anisotropic damage model for alternate/cyclic loading

- Lemaitre and Mazars (1980) **criterion function**

$$f = \varepsilon_{\text{Maz}} - \kappa \leq 0, \qquad \varepsilon_{\text{Maz}} = \sqrt{\langle \boldsymbol{\varepsilon} \rangle^{+} : \langle \boldsymbol{\varepsilon} \rangle^{+}}$$

  $\langle \cdot \rangle^{+}$: positive part of symmetric 2nd order tensor

- **Consolidation function** extended to alternate loading by the active damage concept (Souid et al 2009, Chambart et al, 2010))

$$\kappa = \kappa_0 + S R_v^s \left[(\boldsymbol{H} - \mathbf{1}) : \tilde{\boldsymbol{Q}} \right]^{1/a}, \quad \text{with} \quad \tilde{\boldsymbol{Q}} = \frac{\langle \tilde{\boldsymbol{\varepsilon}} \rangle^{+}}{\max_I \langle \tilde{\varepsilon}_I \rangle}, \quad \tilde{\boldsymbol{\varepsilon}} = \mathbb{E}^{-1} : \boldsymbol{\sigma}$$

  $R_v(\operatorname{tr} \boldsymbol{\sigma} / \sigma_{\text{vM}})$: triaxiality function (and $\sigma_{\text{vM}} = \sqrt{\frac{3}{2} \boldsymbol{\sigma}^D : \boldsymbol{\sigma}^D}$)

- **Damage evolution law**

$$\dot{\boldsymbol{H}} = \dot{\lambda} \frac{\partial \tilde{\varepsilon}_{\text{Maz}}}{\partial \tilde{\boldsymbol{\varepsilon}}} = \dot{\lambda} \frac{\langle \tilde{\boldsymbol{\varepsilon}} \rangle^{+}}{\tilde{\varepsilon}_{\text{Maz}}}$$

- Once $\tilde{\boldsymbol{\sigma}}$ and $\boldsymbol{H}$ are known, computation of the **stress tensor** by

$$\boldsymbol{\sigma} = \boldsymbol{H}^{-1} \cdot \tilde{\boldsymbol{\sigma}} \cdot \boldsymbol{H}^{-1} - \frac{\boldsymbol{H}^{-2} : \tilde{\boldsymbol{\sigma}}}{\operatorname{tr} \boldsymbol{H}^{-2}} \boldsymbol{H}^{-2} + \frac{1}{3} \left[\frac{3 \langle \operatorname{tr} \tilde{\boldsymbol{\sigma}} \rangle}{\operatorname{tr} \boldsymbol{H}^{2}} - \langle - \operatorname{tr} \tilde{\boldsymbol{\sigma}} \rangle \right] \mathbf{1}$$

Non-local damage theory (Pijaudier-Cabot and Bazant, 1987)

- Non-local damage criterion: $f = \varepsilon^{\text{nl}}_{\text{Maz}} - \kappa \leq 0$

- Non-local equivalent strain

$$\varepsilon^{\text{nl}}_{\text{Maz}}(\boldsymbol{x}) = \frac{1}{V_r(\boldsymbol{x})} \int_\Omega \mathcal{W}_0 \left(\frac{\| \boldsymbol{x} - \boldsymbol{\xi} \|}{\ell_{int}} \right) \varepsilon_{\text{Maz}}(\boldsymbol{\xi}) \, \mathrm{d}V_{\boldsymbol{\xi}}$$

$$V_r(\boldsymbol{x}) = \int_\Omega \mathcal{W}_0 \left(\frac{\| \boldsymbol{x} - \boldsymbol{\xi} \|}{\ell_{int}} \right) \mathrm{d}V_{\boldsymbol{\xi}}$$

- **Bump function as weight function** $\mathcal{W}_0(r) = \exp\left(-\frac{1}{\langle 1 - r^2 \rangle} \right)$

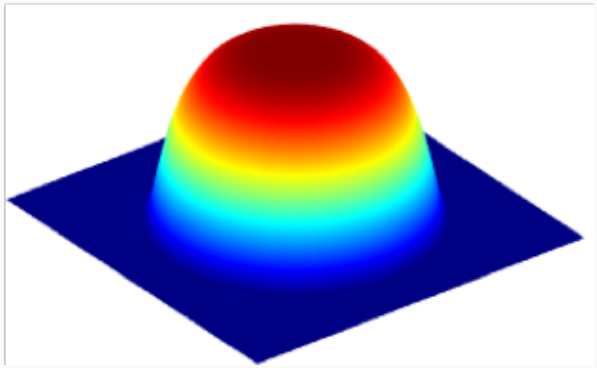

Monotonic and cyclic FE computations of the realistic virtual concrete specimens

Cubic specimens

Virtual concrete specimens $L \times L \times L$ with $L = 10$ cm

- Elastic (undamageable) aggregates, Young's modulus $E = 60\,000$ MPa, Poisson's ratio $\nu = 0.22$.
- Nonlocal anisotropic damage model for the mortar

Table: Material parameters for the mortar

E	v	κ_0	S	s	a	B	ℓ_{int}
30 000 MPa	0.2	$8\ 10^{-5}$	$1.6\ 10^{-4}$	4.18	1.1	1.857	10 mm

Nonlocal internal length $\ell_{int} = L/10 = 10$ mm = specimen size /10

Aggregate size comprised between 8 and 30 mm

$\rightarrow$ the equivalent strain is predominantly weighted from the local equivalent strain of the mortar elements.

Alternate tension-compression-tension-compression

Hysteresis loops and of the cyclic stress softening phenomenon.

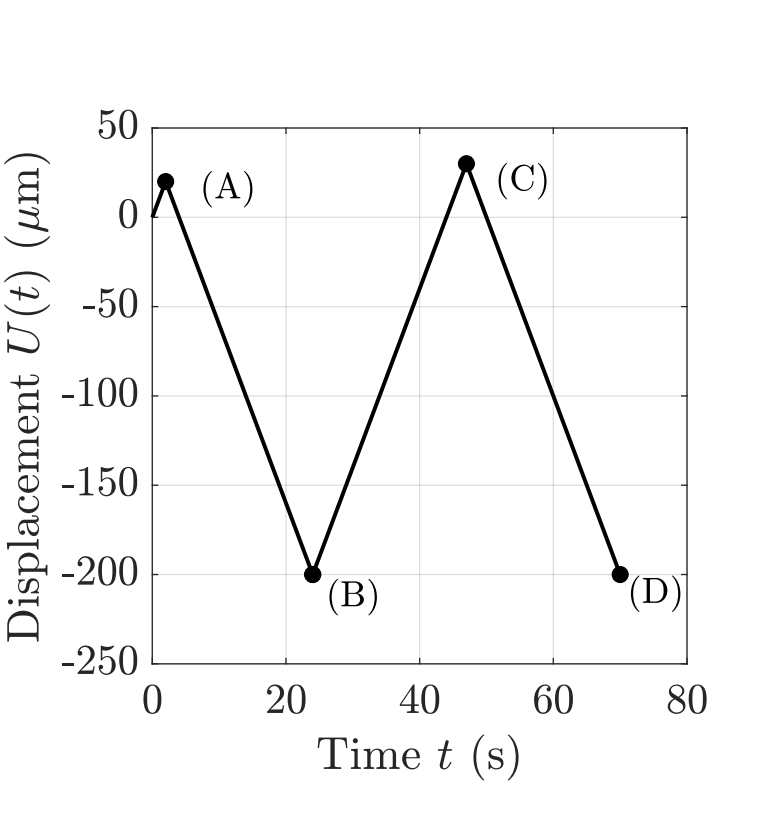

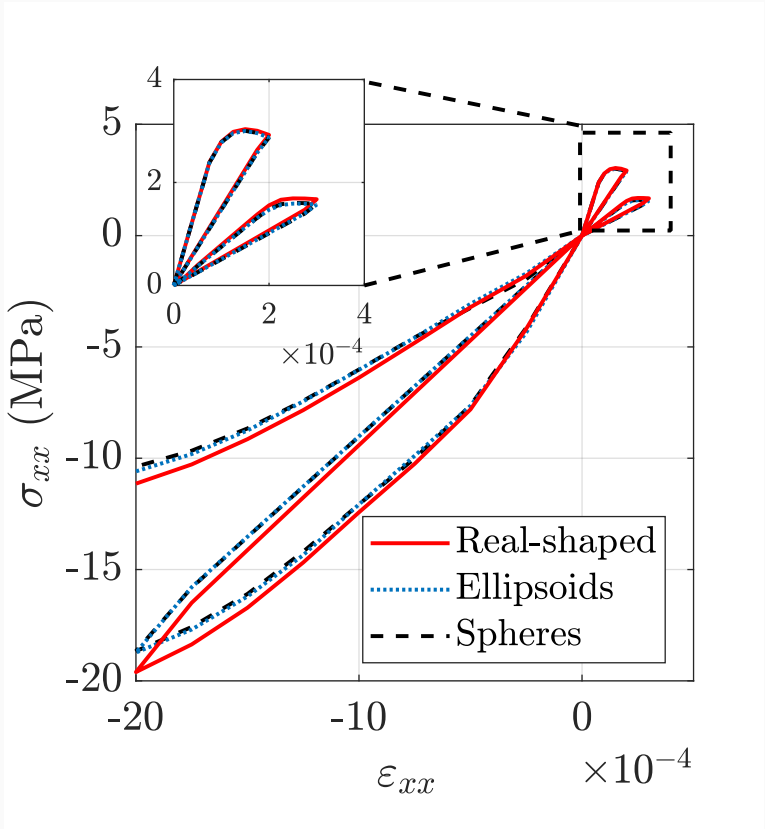

Specimen with real-shaped the most resistant in the compression stages.

More sensitive to aggregate shape in cyclic load. than in monotonic load.

Components D_{ij} for the tension loading at point (A) $U = 20\ \mu$m

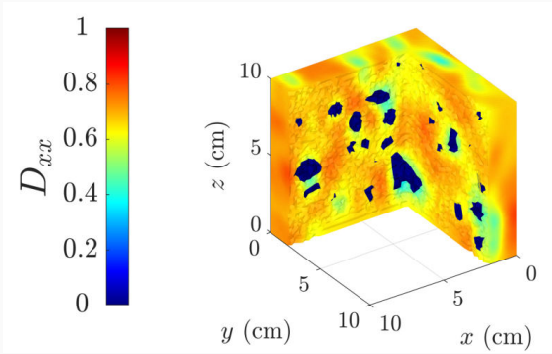

(a) Diagonal damage component D_{xx}.

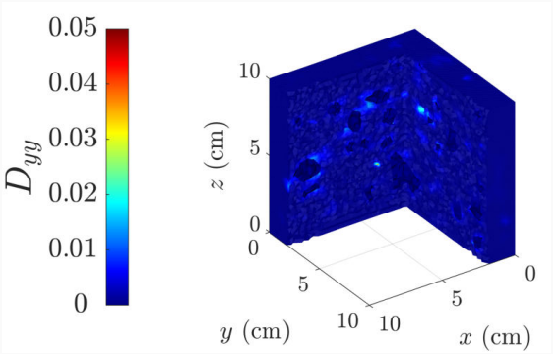

(b) Diagonal damage component D_{yy}.

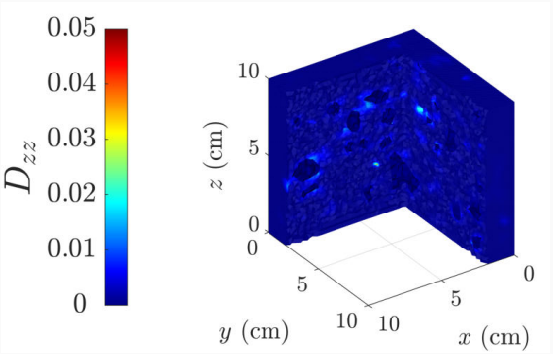

(c) Diagonal damage component D_{zz}.

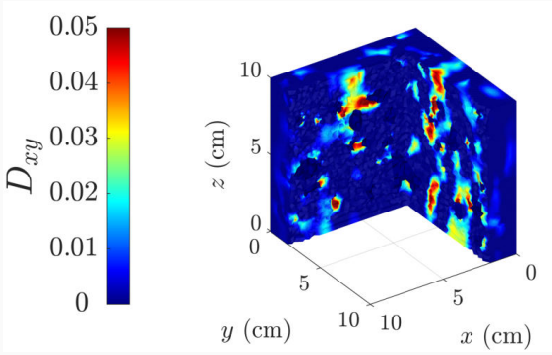

(d) Shear damage component D_{xy}.

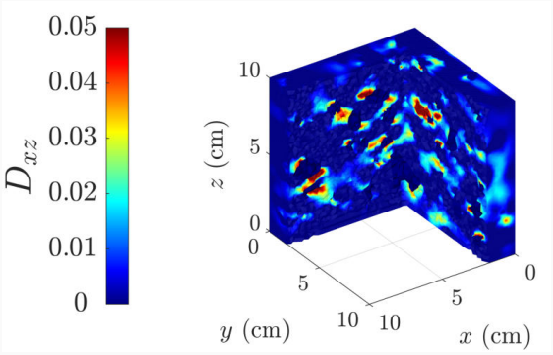

(e) Shear damage component D_{xz}.

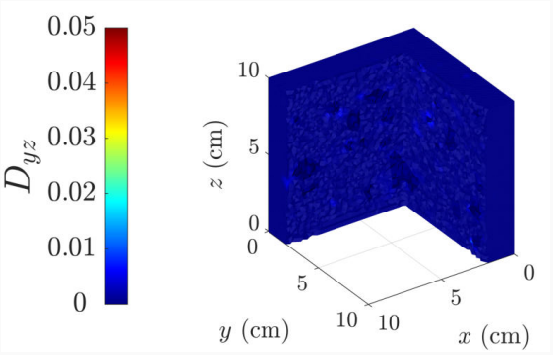

(f) Shear damage component D_{yz}.

Interpretation of anisotropic damage results

Analysis of the damage tensor through the components is not suitable (values depend on the considered working basis)

At a single Gauss point of a structure, a visual possibility of some quantity of interest in direction $\boldsymbol{n}$ is (Rose diagram in 2D) (see Oda, 1982, Kanatani, 1984)

- to set $\boldsymbol{n}$ a vector of the unit sphere
- and to plot and analyze the scalar directional data $f(\boldsymbol{n})$

For continuously damaged materials, the function $f(\boldsymbol{n})$ can be

- the effective Young (resp. shear) modulus $\tilde{E}(\boldsymbol{n})$ (resp. $\tilde{G}(\boldsymbol{n})$) (Ladevèze, 1983),
- the crack density (Lubarda & Krajcinovic 1993,Tikhomirov et al, 2001)

Representation for heterogeneous fields

Such visualizations are not possible for full heterogeneous fields.

Since the damage variable is a symmetric second-order tensor $\boldsymbol{D}$, same possibilities as for the stress tensor:

- maximal principal damage $\max_I D_I$
- some of its invariants

The retained invariants for the stress tensor (von Mises stress σ_{vM}, stress triaxiality...) are **related to plasticity coupled with damage**

Necessary to analyze the induced-damage anisotropy by considering invariants of the damage tensor

$\Rightarrow$ **which invariants are mechanically interesting for pure (anisotropic) damage models ?**

Invariants for analyzing the damage tensor

The damage tensor $\boldsymbol{D}$, of principal damages $D_I \in [0, 1]$, is obtained by post-processing, as $\boldsymbol{D} = \mathbf{1} - \boldsymbol{H}^{-2}$, $D_I = 1 - H_I^{-2}$.

The maximum principal damage $\max D_I$ is naturally plotted as the main indicator of the location of the further macroscopic crack.

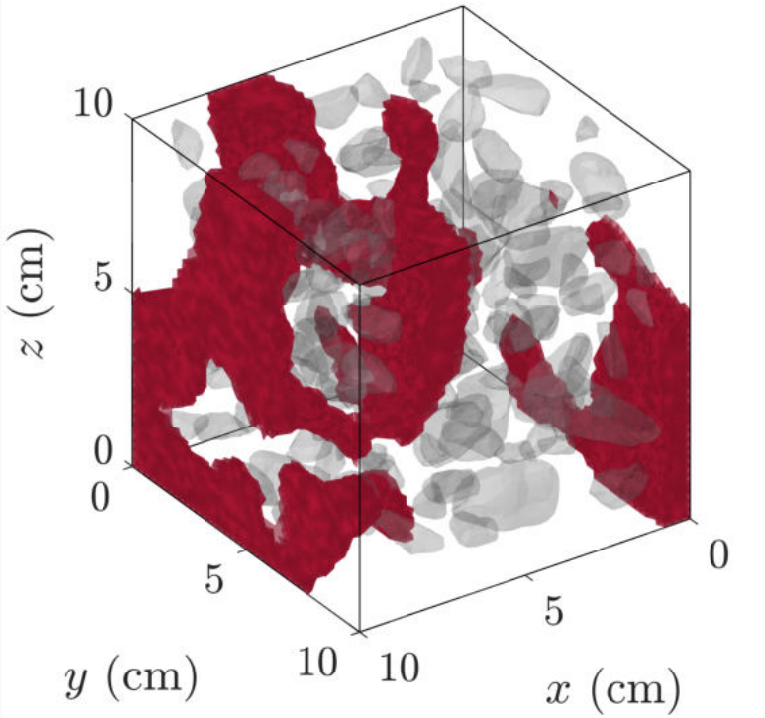

Domain of maximum principal damage $\max D_I > 0.96$ at the end of tension

Distance to isotropy

- **of the damage tensor D,**
- **of the effective (damaged) compliance tensor $\tilde{\mathbb{S}}$**

Distance to isotropy of the symmetric 2nd order damage tensor

Harmonic decomposition = hydrostatic/deviatoric decomposition

$$\boldsymbol{D} = \frac{1}{3}\,(\mathrm{tr}\,\boldsymbol{D})\,\mathbf{1} + \boldsymbol{D}^D,$$

such that

$\| \boldsymbol{D} \|^2 = \boldsymbol{D} : \boldsymbol{D} = \| \frac{1}{3}\,\mathrm{tr}\,\boldsymbol{D}\,\mathbf{1} \|^2 + \| \boldsymbol{D}^D \|^2 = \frac{1}{3}(\mathrm{tr}\,\boldsymbol{D})^2 + \| \boldsymbol{D}^D \|^2.$

The distance $d(\boldsymbol{D}, \text{isotropy})$ of the damage tensor to isotropy is the minimum of the distance between $\boldsymbol{D}$ and the isotropic tensor

$$\boldsymbol{D}^* = \frac{1}{3}\alpha^*\,\mathbf{1}$$

$$\begin{aligned} d(\boldsymbol{D}, \text{isotropy})^2 = \min_{\boldsymbol{D}^* \text{ isotropic}} \| \boldsymbol{D} - \boldsymbol{D}^* \|^2 &= \min_{\alpha^*} \| \boldsymbol{D} - \frac{1}{3}\alpha\mathbf{1} \|^2 \\ &= \min_{\alpha^*} \left(\frac{1}{3}\,(\mathrm{tr}\,\boldsymbol{D} - \alpha^*)^2 + \| \boldsymbol{D}^D \|^2 \right) \\ &= \| \boldsymbol{D}^D \|^2, \end{aligned}$$

since the minimum is provided by $\alpha^* = \mathrm{tr}\,\boldsymbol{D}$.

$D_{\text{vM}} = \sqrt{\frac{3}{2}\boldsymbol{D}^D : \boldsymbol{D}^D}$ = distance to isotropy of the damage tensor

The isotropic part of $\boldsymbol{D}$ is therefore the orthogonal projection on the vector space of isotropic tensors (spanned by $\mathbf{1}/\sqrt{3}$),

$$\boldsymbol{D}^{\text{iso}} = \frac{1}{3}\,(\text{tr}\,\boldsymbol{D})\,\mathbf{1}. \tag{1}$$

A distance of damage $\boldsymbol{D}$ to isotropy is either[1]

$$d(\boldsymbol{D}, \text{isotropy}) = \parallel \boldsymbol{D}^D \parallel = \sqrt{\frac{2}{3}}\, D_{\text{vM}}, \tag{2}$$

or simply D_{vM}.

$\Rightarrow$ The von Mises equivalent damage $D_{\text{vM}} = \sqrt{\frac{3}{2}} \parallel \boldsymbol{D}^D \parallel$
can be **interpreted as a distance to (damage) isotropy**.

[1] $\boldsymbol{D}^D = \boldsymbol{D} - \frac{1}{3}\,\text{tr}\,\boldsymbol{D}\,\mathbf{1}$: deviatoric part of 2nd order tensor $\boldsymbol{D}$

Case of elasticity (or compliance) tensors $\hat{\mathbb{E}}$

We recall that

$$\mathbb{E}\mathrm{la} = \left\{ \hat{\mathbb{E}} \text{ fourth order tensor, } \hat{E}_{ijkl} = \hat{E}_{ijlk} = \hat{E}_{jikl} = \hat{E}_{klij} \right\}$$

is the vector space of elasticity tensors.

- The distance $d(\hat{\mathbb{E}}, \text{isotropy})$ of $\hat{\mathbb{E}}$ to isotropy is obtained by orthogonal projection on the vector space of isotropic tensors (Vianello, 1997).
- We calculate $d(\hat{\mathbb{E}}, \text{isotropy})$ with 3D formulas from Abramian (2020) related to the harmonic decomposition of elasticity tensors.

We define the (3D) deviatoric projector

$$\mathbb{J} = \mathbb{I} - \frac{1}{3}\mathbf{1} \otimes \mathbf{1}$$

the fourth order tensor $\mathbb{J} \in \mathbb{E}\mathrm{la}$ such as $\boldsymbol{D}^D = \mathbb{J} : \boldsymbol{D}$

Isotropic part of an elasticity (or compliance) tensor $\hat{\mathbb{E}}$

Let $\hat{\mathbb{E}}$ be a possibly anisotropic elasticity or compliance tensor

One can decompose $\hat{\mathbb{E}}$ as its isotropic part + its anisotropic part,

$$\hat{\mathbb{E}} = \hat{\mathbb{E}}^{\text{iso}} + \hat{\mathbb{E}}^{\text{aniso}}, \qquad \hat{\mathbb{E}}^{\text{iso}} :: \hat{\mathbb{E}}^{\text{aniso}} = 0,$$

where **the isotropic part of $\hat{\mathbb{E}}$ is**

$$\hat{\mathbb{E}}^{\text{iso}} = 2\hat{G}\,\mathbb{J} + \hat{K}\,\mathbf{1}\otimes\mathbf{1}, \qquad \begin{cases} 2\hat{G} = \frac{1}{5}\,\hat{\mathbb{E}} :: \mathbb{J} = \frac{1}{15}\left(3\,\mathrm{tr}\,\hat{\boldsymbol{v}} - \mathrm{tr}\,\hat{\boldsymbol{d}}\right), \\ 3\hat{K} = \frac{1}{3}\,\mathbf{1} : \hat{\mathbb{E}} : \mathbf{1} = \frac{1}{3}\,\mathrm{tr}\,\hat{\boldsymbol{d}} \end{cases}$$

with (dilatation second order tensor)

$$\hat{\boldsymbol{d}} = \boldsymbol{d}(\hat{\mathbb{E}}) = \mathrm{tr}_{12}\,\hat{\mathbb{E}} \qquad (\hat{d}_{ij} = \hat{E}_{kkij})$$

and (Voigt second order tensor)

$$\hat{\boldsymbol{v}} = \boldsymbol{v}(\hat{\mathbb{E}}) = \mathrm{tr}_{13}\,\hat{\mathbb{E}} \qquad (\hat{v}_{ij} = \hat{E}_{kikj})$$

Distance to isotropy of an elasticity/compliance-type tensor $\hat{\mathbb{E}}$

The distance $d(\hat{\mathbb{E}}, \text{isotropy})$ of the elasticity tensor $\hat{\mathbb{E}}$ to isotropy is then obtained as the minimum for $G^* = \hat{G}$ and $K^* = \hat{K}$:

$$
\begin{aligned}
d(\hat{\mathbb{E}}, \text{isotropy})^2 &= \min_{\substack{\mathbb{E}^* \\ \text{isotropic}}} \| \hat{\mathbb{E}} - \mathbb{E}^* \|^2 \\
&= \min_{G^*, K^*} \| \hat{\mathbb{E}} - (2G^* \, \mathbb{J} + K^* \, \mathbf{1} \otimes \mathbf{1}) \|^2 \\
&= \min_{G^*, K^*} \left(\| \hat{\mathbb{E}}^{\text{iso}} - (2G^* \, \mathbb{J} + K^* \, \mathbf{1} \otimes \mathbf{1}) \|^2 \right) + \| \hat{\mathbb{E}}^{\text{aniso}} \|^2 \\
&= \| \hat{\mathbb{E}}^{\text{aniso}} \|^2 \\
&= \| \hat{\mathbb{E}} - \hat{\mathbb{E}}^{\text{iso}} \|^2
\end{aligned}
$$

The distance to isotropy of $\hat{\mathbb{E}}$ is

$$
d(\hat{\mathbb{E}}, \text{isotropy}) = \| \hat{\mathbb{E}} - \hat{\mathbb{E}}^{\text{iso}} \|
$$

Retained indicator of damage-induced anisotropy

Let $\tilde{\mathbb{S}} \in \mathbb{E}\mathrm{la}$ be the effective (damaged) compliance tensor

such that elasticity law recasts $\boldsymbol{\varepsilon} = \tilde{\mathbb{S}} : \boldsymbol{\sigma}$.

The relative distance to isotropy of $\tilde{\mathbb{S}}$ is

$$\delta_{\tilde{\mathbb{S}}} = \frac{d(\tilde{\mathbb{S}}, \text{isotropy})}{\| \tilde{\mathbb{S}}^{iso} \|} = \frac{\| \tilde{\mathbb{S}} - \tilde{\mathbb{S}}^{iso} \|}{\| \tilde{\mathbb{S}}^{iso} \|}$$

$\delta_{\tilde{\mathbb{S}}}$ is the distance of $\tilde{\mathbb{S}}$ to isotropy normalized by the norm of its closest isotropic compliance tensor

$$\tilde{\mathbb{S}}^{iso} = \frac{1}{2\tilde{G}} \mathbb{J} + \frac{1}{9\tilde{K}} \mathbf{1} \otimes \mathbf{1}$$

- The relative distance to isotropy $\delta_{\tilde{\mathbb{S}}}$ is dimensionless.
- It assesses the damage-induced anisotropy.
- Contrary to the maximum principal damage $\max_I D_I$, it is independent of the loading intensity.

For our anisotropic damage model

The effective shear and bulk moduli of this isotropic part are

$$\tilde{G} = \frac{30\,G}{3(\operatorname{tr}\boldsymbol{H})^2 + \operatorname{tr}\boldsymbol{H}^2} \qquad \text{and} \qquad \begin{cases} \tilde{K} = \dfrac{3K}{\operatorname{tr}\boldsymbol{H}^2} & \text{if} \quad \operatorname{tr}\boldsymbol{\sigma} > 0, \\ \tilde{K} = K & \text{if} \quad \operatorname{tr}\boldsymbol{\sigma} < 0, \end{cases}$$

$d(\tilde{\mathbb{S}}, \text{isotropy})$ can be expressed as

$$d(\tilde{\mathbb{S}}, \text{isotropy}) = \parallel \tilde{\mathbb{S}} - \tilde{\mathbb{S}}^{iso} \parallel = \sqrt{\tilde{\mathbb{S}} :: \tilde{\mathbb{S}} - \frac{5}{4\tilde{G}^2} - \frac{1}{9\tilde{K}^2}}.$$

Alternate tension-compression-tension-compression

Hysteresis loops and of the cyclic stress softening phenomenon.

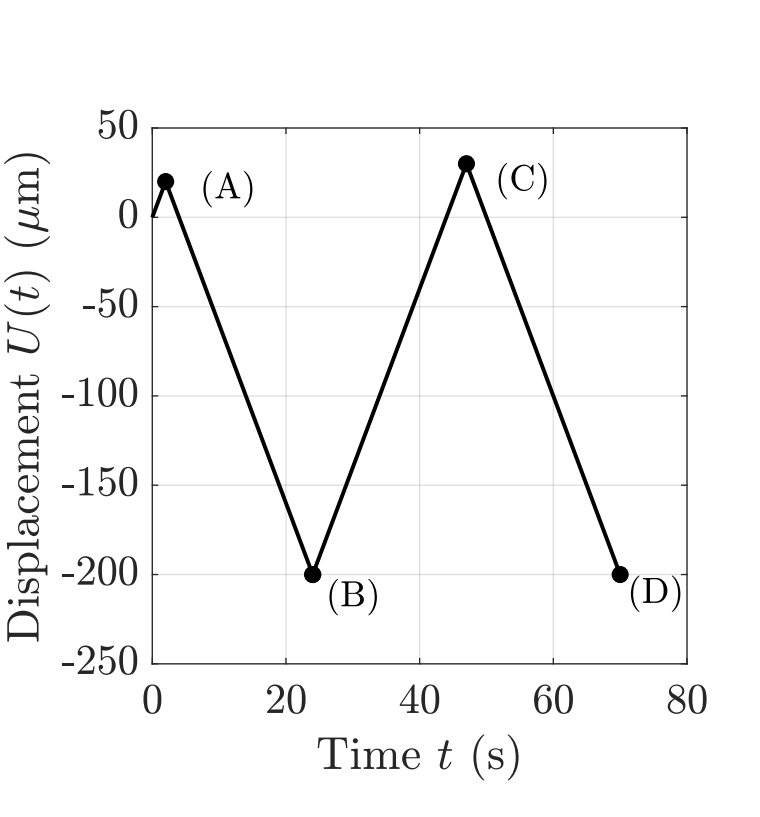

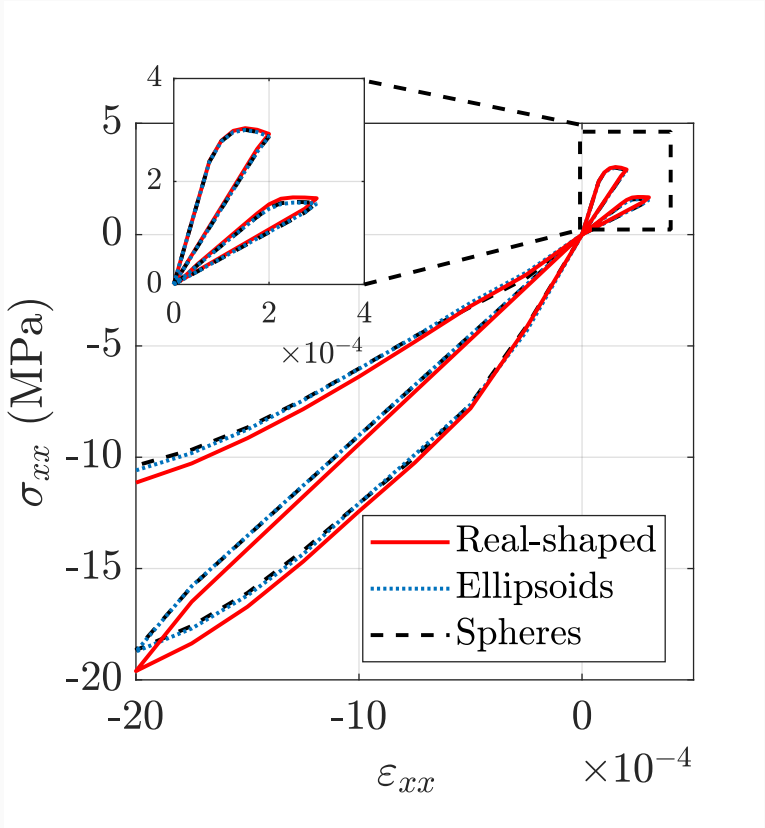

Specimen with real-shaped the most resistant in the compression stages.

More sensitive to aggregate shape in cyclic load. than in monotonic load.

Damage indicators in alternate loading

Always increasing maximum principal damage
(since $\boldsymbol{D} = \mathbf{1} - \boldsymbol{H}^{-2}$, $\dot{\boldsymbol{H}} \geq 0 \implies \dot{\boldsymbol{D}} \geq 0 \implies \frac{\mathrm{d}}{\mathrm{d}t} \max_I D_I$)

But non-monotonic evolution of the damage-induced anisotropy

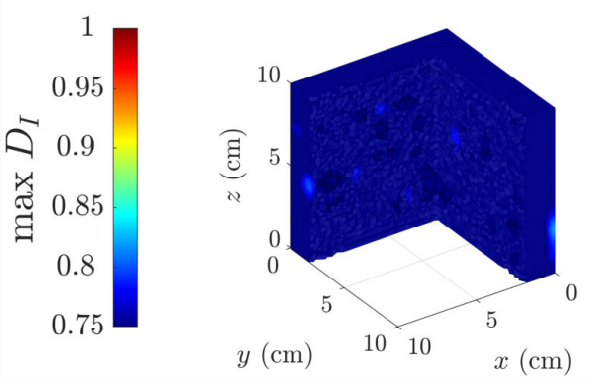

(a) Point (A) - tension

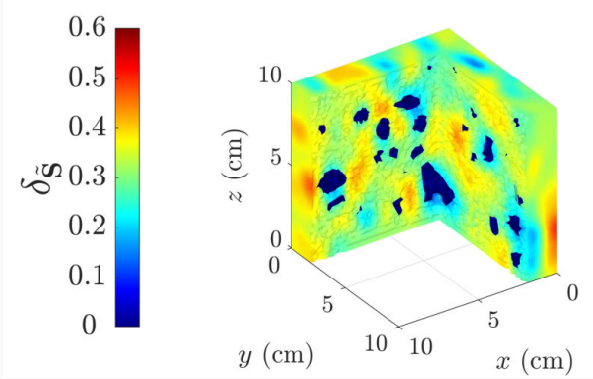

(b) $\delta_{\tilde{\mathbb{S}}}$ point (A) - tension

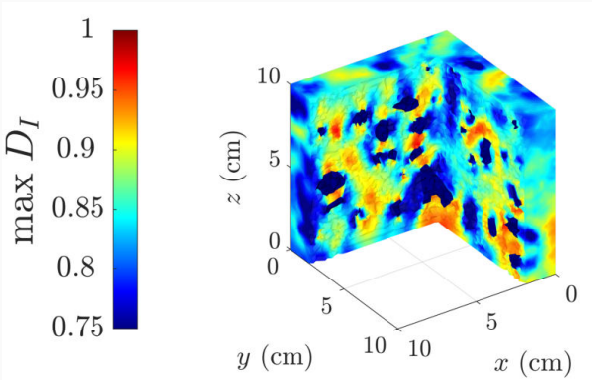

(c) Point (B)- compression

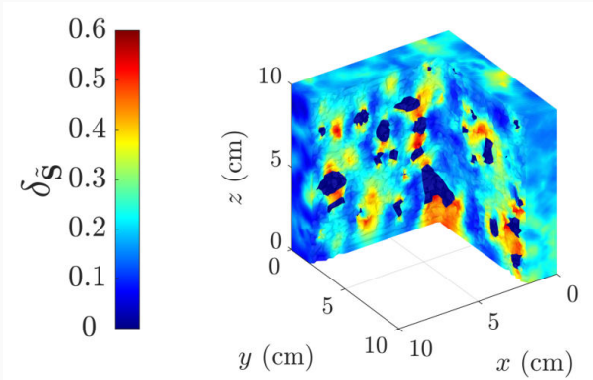

(d) $\delta_{\tilde{\mathbb{S}}}$ point (B)- compression

Damage indicators in alternate loading

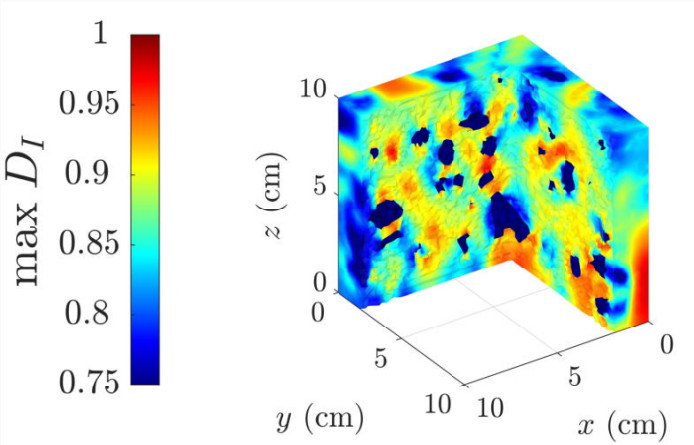

(a) Point(C) - 2nd tension

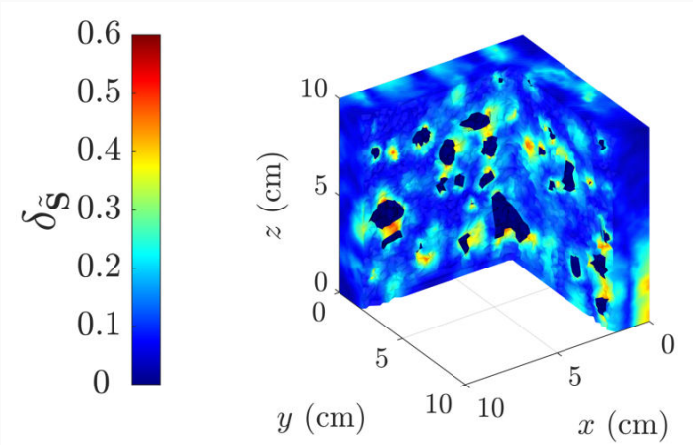

(b) $\delta_{\tilde{\mathbb{S}}}$ point (C) - 2nd tension

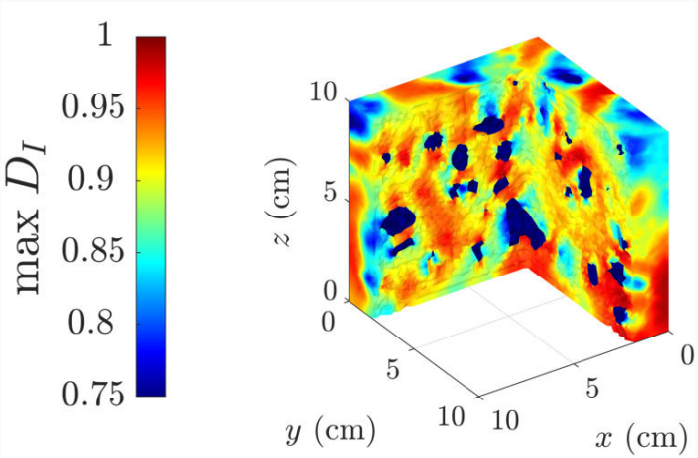

(c) Point (D) - 2nd compression

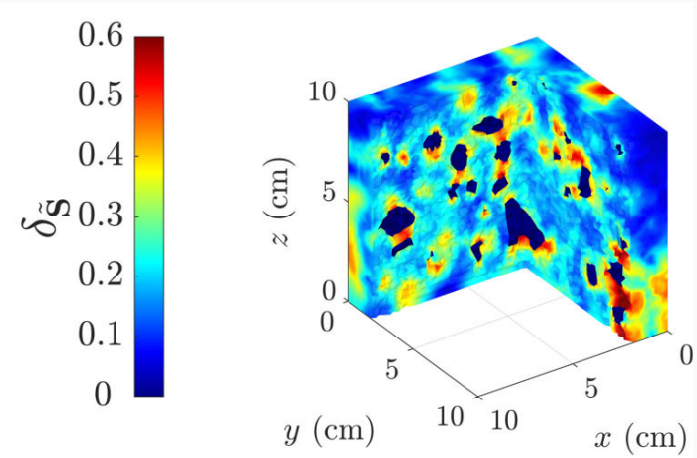

(d) $\delta_{\tilde{\mathbb{S}}}$ point (D) - 2nd compression

Conclusion

Conclusion

High model complexity (laser-scanned aggregates, nonlocal anisotropic damage, cyclic loading) can be handled in mesostructures computations.

Constitutive model and its 3D numerical implementation robust, up to high levels of damage.

Tensorial damage (and $\max_I D_I$) increases within the mortar matrix, while damage-induced anisotropy may increase and decrease.

Plotting (relative) distances to isotropy provides complementary information over the whole structure

Supplement

Representing damage for cyclic cases

Concrete modelling with idealised aggregate shapes such as spheres is nowadays common since Wriggers and Moftah (2004)

- representation of spheres by their centre and radius helps to avoid overlapping particles analytically.
- ellipsoidal aggregate shapes (Liu et al, 2014, Wang et al, 2015),
- experimental data extracted from tomography images (Huang et al, 2015, Mazzucco et al, 2020) or laser scanning techniques combined with image analysis (Fernlund, 2005, Mazzucco et al, 2018, Thilakarathna et al, 2021) can now be exploited.

Representing damage for mesoscale concrete specimens

Two-component modelling:

- Elastic aggregates with real shapes
- Damaging mortar
  - Most models dedicated to either compression or tension loading
  - Representing properly the difference in behavior of cementitious materials between tension and compression requires anisotropic damage
  - Dedicated model for representing cyclic/alternate loading cases
  - Permanent strains are neglected (Lemaitre and Mazars, 1980, Mazars, 1984, Mazars and Pijaudier-Cabot, 1989).

Placement of an aggregate

- As soon as a separating axis is found (in practice among 15), there is no overlapping between the OBBs; the placement of the aggregate with respect to this criterion is accepted.

- If all candidate axes are tested without finding a separating axis, the OBBs are considered to overlap, the new aggregate is repositioned randomly.

- The procedure is repeated iteratively until a collision-free arrangement is obtained.

Overlapping OBBs

Checking the non overlapping of aggregates as non overlapping of oriented bounding boxes is a conservative procedure.

OBBs can intersect, without necessarily the aggregates themselves intersecting.

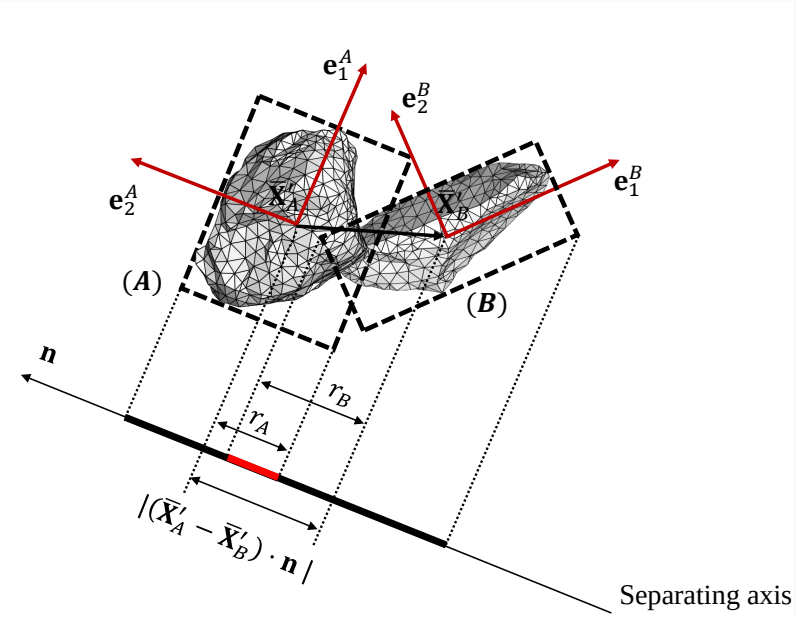

(a)

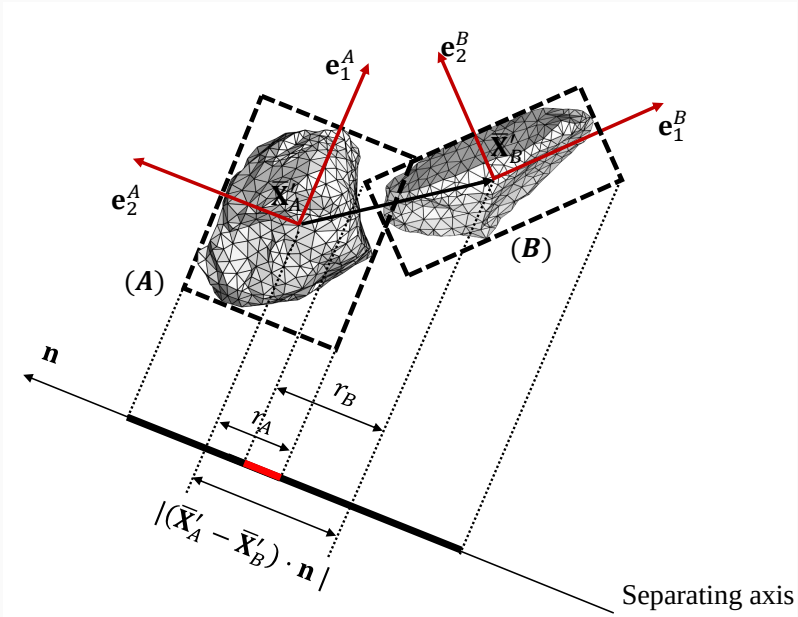

(b)

Two scenarios of OBBs overlapping,
(a) OBBs and aggregates overlap, (b) OBBs overlap but aggregates do not

Algorithm to generate heterogeneous specimen geometries

Inputs: aggregates geometries, maximum element size h_{max}, target volume fraction ϕ_{ag} and sieve segments $[d_0, d_1[, \ldots, [d_{B-1}, d_B[$.

1. Mesh the retained laser-scanned aggregates.
2. Calculate the maximum principal length d, the reference bounding box and the volume v_{ag} of each aggregate.
3. Sort the aggregates according to the B sieve segments $[d_0, d_1[, \ldots, [d_{B-1}, d_B[$.

4. Loop over the batch b of aggregates in a sieve segment $[d_{B-b}, d_{B-b+1}[$, from $b = 1$ to $b = B$.
   - 4.1 Calculate the target volume $V_{ag}(d_{B-b}, d_{B-b+1})$ of the sieve segment.
   - 4.2 Randomly pick an aggregate j (of volume v_{ag}^{j}) in the sieve segment.
   - 4.3 Randomly place the aggregate j inside the specimen.
   - 4.4 If the aggregate j crosses the specimen boundaries then reject it and go back to (b).
   - 4.5 Compute its Oriented Bounding Box (OBB_j).
   - 4.6 If its OBB_j overlaps another aggregate OBB_k then reject it and go back to (b). If not, accept it at its place in the concrete specimen.
   - 4.7 Update the volume $V_{ag}^{j} = V_{ag}^{j-1} + v_{ag}^{j}$ of placed aggregates. Loop for batch b (go to 5) as long as $V_{ag}^{j} < V_{ag}\left(d_{B-1}, d_{B}\right) + \ldots + V_{ag}\left(d_{B-b}, d_{B+1-b}\right)$.
5. Mesh the virtual concrete specimen.

Output: FE mesh of the aggregate-mortar mesostructure.

Mesoscale model for concrete

Concrete, a quasi-brittle composite material comprising

- mortar
- aggregates

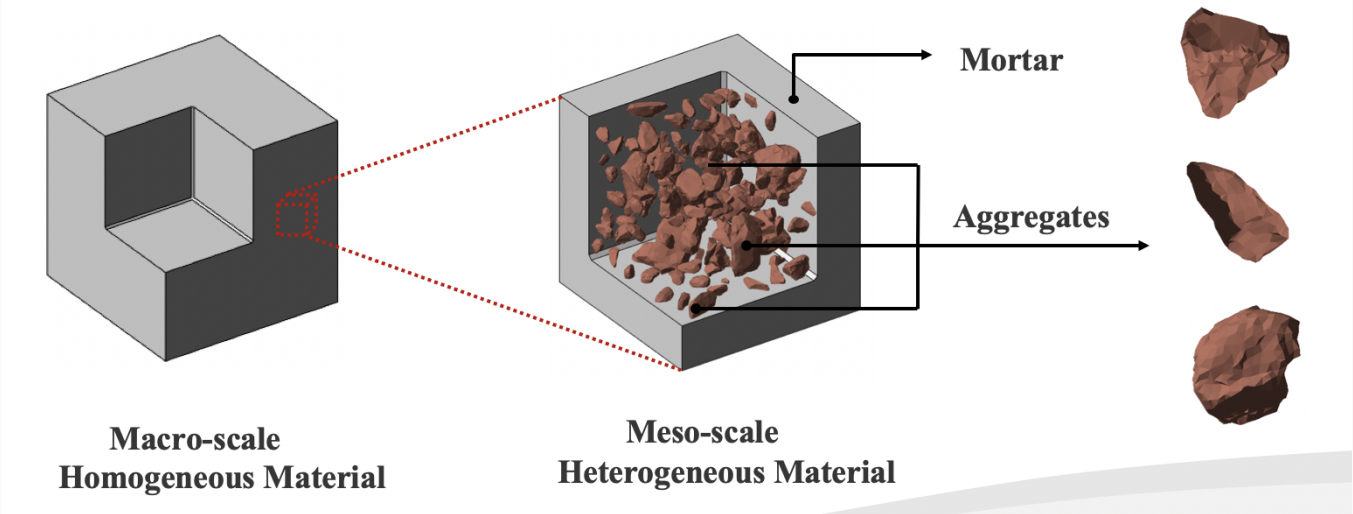

Loss of bearing capacity described by Continuum Damage Mechanics

- Isotropic damage described by a scalar variable
- Anisotropy of the micro-cracking pattern oriented by the loading
  $\Rightarrow$ Anisotropic damage described by a tensorial variable

Numerical Scheme (1-Elastic Prediction)

Inputs: ε_{n+1}, $\tilde{\varepsilon}_n$, $\boldsymbol{H}_n$ (and $\boldsymbol{D}_n$), and $T_{X\,n}$.

- Compute R_{vn}, $\varepsilon_{I\,n+1}$,

$$\varepsilon_{\text{Maz}\,n+1} = \sqrt{\sum_I \langle \varepsilon_{I\,n+1} \rangle^2}, \quad \tilde{\varepsilon}_{I\,n} \quad \text{and} \quad \tilde{\varepsilon}_{\text{Maz}\,n} = \sqrt{\sum_I \langle \tilde{\varepsilon}_{I\,n} \rangle^2}$$

- If either $\varepsilon_{\text{Maz}\,n+1} = 0$ or $\tilde{\varepsilon}_{\text{Maz}\,n} = 0$ then $f^{\text{try}} = -\kappa_0$.
- Else:
  (i) determine

$$\tilde{\boldsymbol{P}}_n = \frac{\langle \tilde{\boldsymbol{\varepsilon}}_n \rangle^+}{\tilde{\varepsilon}_{\text{Maz}\,n}}, \qquad \boldsymbol{P}_{n+1} = \frac{\langle \boldsymbol{\varepsilon}_{n+1} \rangle^+}{\varepsilon_{\text{Maz}\,n+1}}, \qquad \tilde{\boldsymbol{Q}}_n = \frac{\langle \tilde{\boldsymbol{\varepsilon}}_n \rangle^+}{\max_I \langle \tilde{\varepsilon}_{I\,n} \rangle}$$

  (ii) calculate $f^{\text{try}} = \varepsilon^{\text{nl}}_{\text{Maz}\,n+1} - \kappa^{\text{try}}$ for the non-local model, where

$$\kappa^{\text{try}} = \kappa_0 + SR^s_{vn} \left[(\boldsymbol{H}_n - \boldsymbol{1}) : \tilde{\boldsymbol{Q}}_n \right]^{1/a}$$

Numerical Scheme (2-Damage update)

- If $f^{\text{try}} \leq 0$, then

$$\boldsymbol{H}_{n+1} = \boldsymbol{H}_n \qquad (\text{and } \boldsymbol{D}_{n+1} = \boldsymbol{D}_n)$$

Else :

$$\Delta\lambda = \frac{\left\langle \mathcal{F} - (\boldsymbol{H}_n - \mathbf{1}) : \tilde{\boldsymbol{Q}}_n \right\rangle}{\tilde{\boldsymbol{P}}_n : \tilde{\boldsymbol{Q}}_n}, \qquad \mathcal{F} = \left\langle \frac{\varepsilon^{\text{nl}}_{\text{Maz}\,n+1} - \kappa_0}{SR^s_{v\,n}} \right\rangle^a,$$

and

$$\boldsymbol{H}_{n+1} = \boldsymbol{H}_n + \Delta\lambda\, \tilde{\boldsymbol{P}}_n \qquad (\text{and } \boldsymbol{D}_{n+1} = \mathbf{1} - \boldsymbol{H}^{-2}_{n+1})$$

Numerical Scheme (3-Stresses and effective strain update)

- Calculate $\tilde{\boldsymbol{\sigma}}_{n+1} = 2G\,\boldsymbol{\varepsilon}_{n+1} + \left(K - \frac{2}{3}G\right) \operatorname{tr}\boldsymbol{\varepsilon}_{n+1}\,\mathbf{1}$ and then

$$\begin{aligned}\boldsymbol{\sigma}_{n+1} =& \boldsymbol{H}_{n+1}^{-1} \cdot \tilde{\boldsymbol{\sigma}}_{n+1} \cdot \boldsymbol{H}_{n+1}^{-1} - \frac{\boldsymbol{H}_{n+1}^{-2} : \tilde{\boldsymbol{\sigma}}_{n+1}}{\operatorname{tr}\boldsymbol{H}_{n+1}^{-2}}\, \boldsymbol{H}_{n+1}^{-2} \\ &+ \frac{1}{3}\left[\frac{3\langle \operatorname{tr}\tilde{\boldsymbol{\sigma}}_{n+1}\rangle}{\operatorname{tr}\boldsymbol{H}_{n+1}^{2}} - \langle -\operatorname{tr}\tilde{\boldsymbol{\sigma}}_{n+1}\rangle\right]\,\mathbf{1}\end{aligned}$$

- Update the stress triaxiality $T_{X\,n+1} = \sigma_{H\,n+1}/\sigma_{\mathrm{vM}\,n+1}$ from $\boldsymbol{\sigma}_{n+1}$.
- Update the effective strain

$$\tilde{\varepsilon}_{n+1} = \frac{1}{2G}\boldsymbol{\sigma}_{n+1} + \frac{1}{3}\left(\frac{1}{3K} - \frac{1}{2G}\right)\operatorname{tr}\boldsymbol{\sigma}_{n+1}\,\mathbf{1}$$

Outputs: $\boldsymbol{\sigma}_{n+1}$, $\tilde{\varepsilon}_{n+1}$, $\boldsymbol{H}_{n+1}$, (and $\boldsymbol{D}_{n+1}$), $T_{X\,n+1}$ and $\mathbb{L}^{c}_{n+1} = \dfrac{\partial \boldsymbol{\sigma}_{n+1}}{\partial \boldsymbol{\varepsilon}_{n+1}}$

Indicators for simple monotonic loadings

Loadings

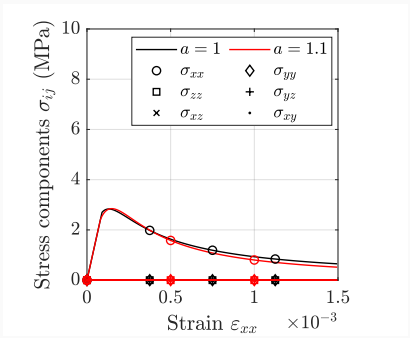

(a) uniaxial tension

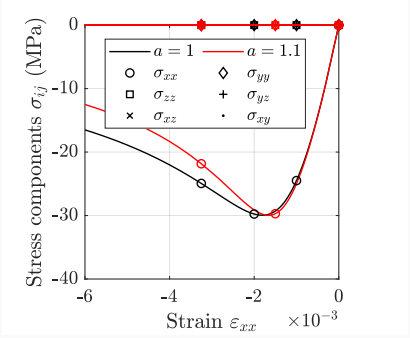

(b) uniaxial compression

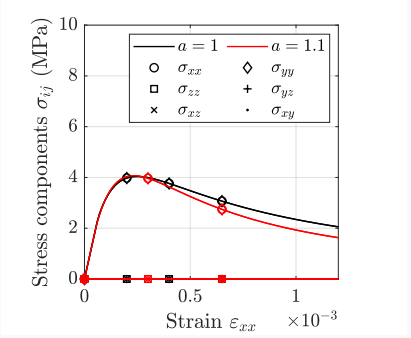

(c) equi-biaxial tension

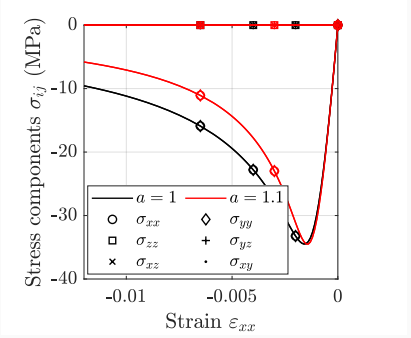

(d) equi-biaxial compression

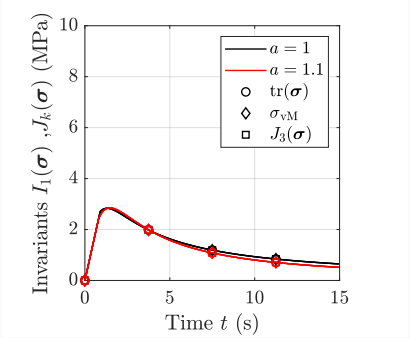

(e) uniaxial tension

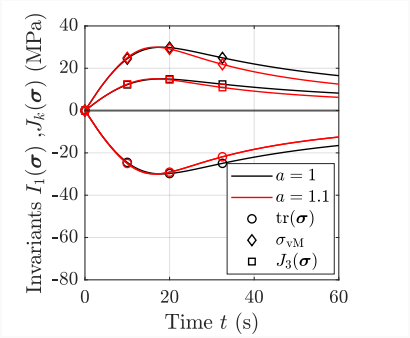

(f) uniaxial compression

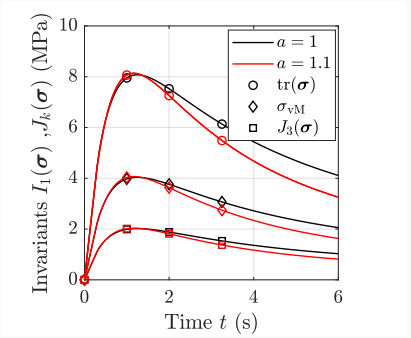

(g) equi-biaxial tension

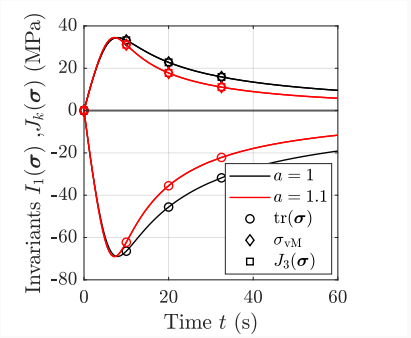

(h) equi-biaxial compression

Ladevèze variable

Second-order symmetric tensor $\boldsymbol{H} = (\mathbf{1} - \boldsymbol{D})^{-\frac{1}{2}}$
used for defining the evolution law

- 6 components: depend on the basis,
- 3 principal values
- 3 invariants:
  - $I_1(\boldsymbol{H}) = \operatorname{tr} \boldsymbol{H}$,
  - $J_2(\boldsymbol{H}) = \sqrt{\frac{3}{2} \boldsymbol{H}^D : \boldsymbol{H}^D}$,
  - $J_3(\boldsymbol{H}) = \left(\frac{27}{2} \det \boldsymbol{H}^D \right)^{1/3}$,

Ladevèze variable

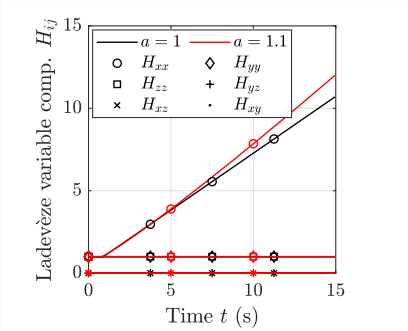

(a) uniaxial tension

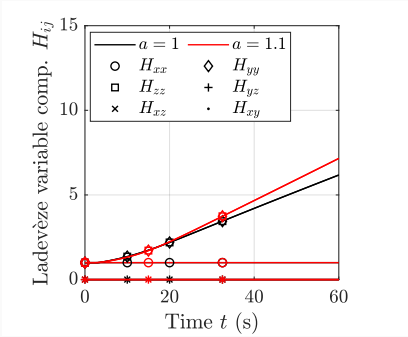

(b) uniaxial compression

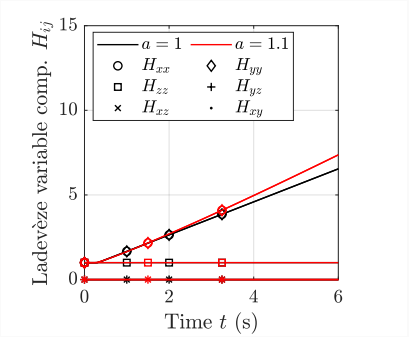

(c) equi-biaxial tension

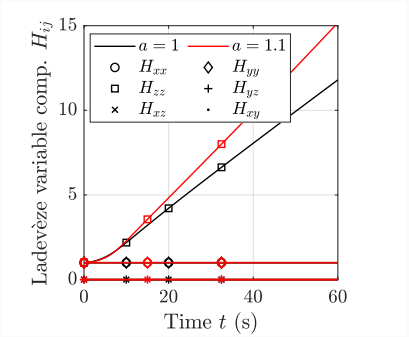

(d) equi-biaxial compression

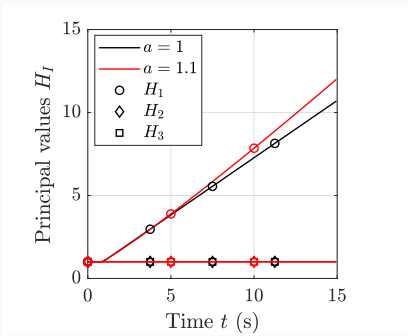

(e) uniaxial tension

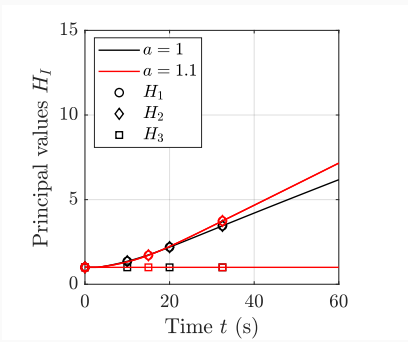

(f) uniaxial compression

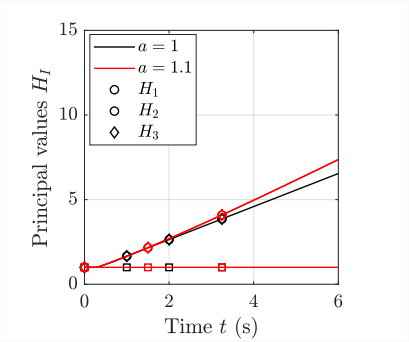

(g) equi-biaxial tension

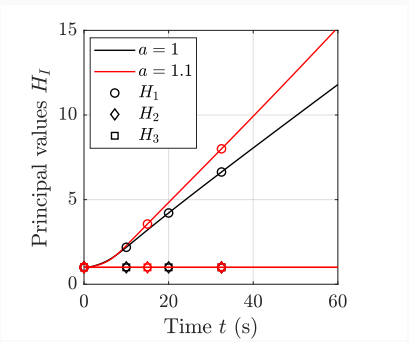

(h) equi-biaxial compression

Damage variable

Second-order symmetric tensor:

- 6 components: depend on the basis,
- 3 principal values
- 3 invariants:
  - $I_1(\boldsymbol{D}) = \operatorname{tr} \boldsymbol{D}$,
  - $J_2(\boldsymbol{D}) = \sqrt{\frac{3}{2} \boldsymbol{D}^D : \boldsymbol{D}^D}$,
  - $J_3(\boldsymbol{D}) = \left(\frac{27}{2} \det \boldsymbol{D}^D \right)^{1/3}$,

Damage $\boldsymbol{D}$ is isotropic if and only if its deviatoric part vanishes ($\boldsymbol{D}^D = 0$).

Damage variable

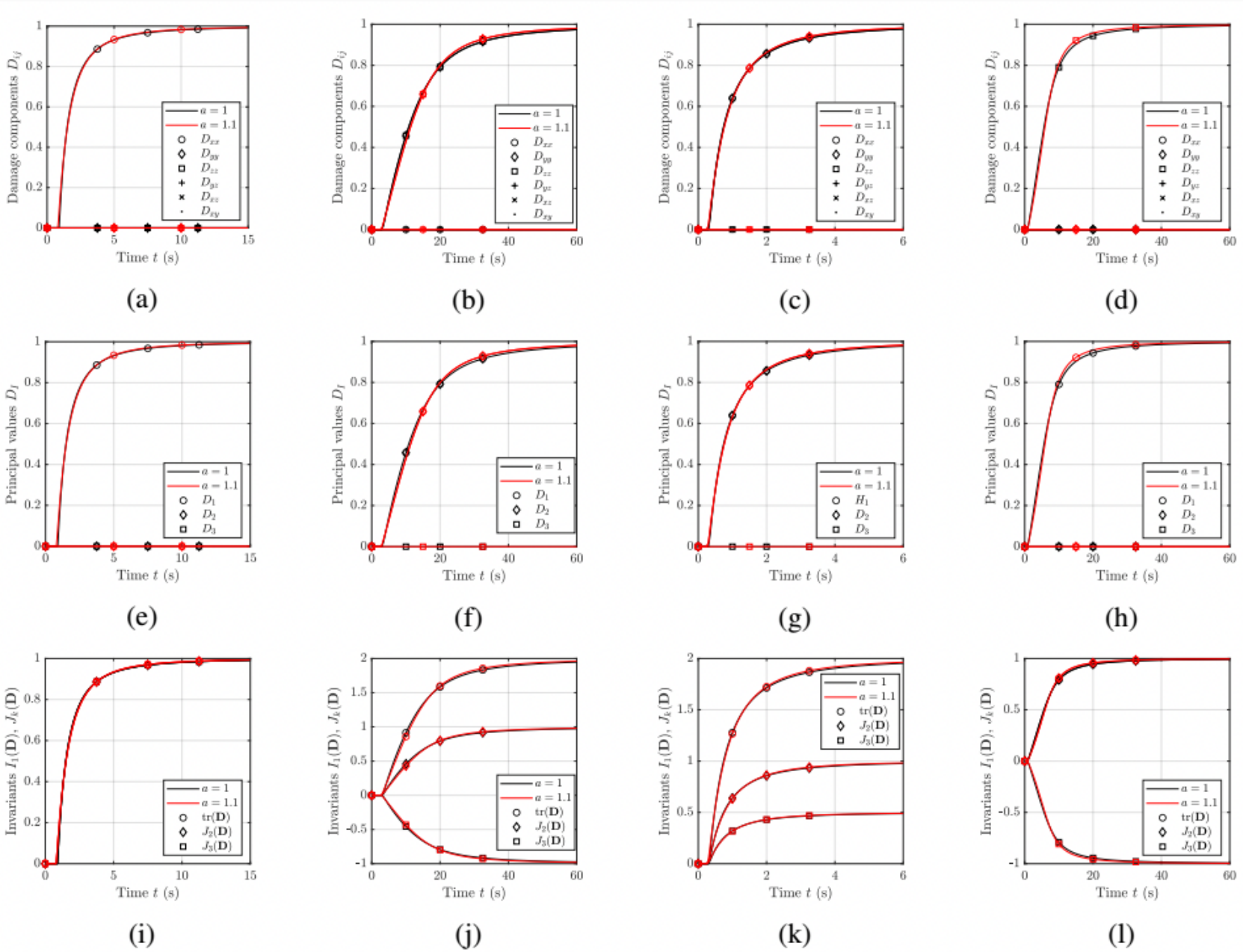

Representation for heterogeneous fields

- The deviatoric part of the damage tensor may vanish (in case of isotropic damage $\boldsymbol{D}^D = 0$, $D_{\text{vM}} = 0$): the standard formulas for stress triaxiality and stress Lode parameter

$$T_X = \frac{1}{3}\frac{\operatorname{tr}\boldsymbol{\sigma}}{\sigma_{\text{vM}}}, \qquad L = \frac{27}{2}\frac{\det\boldsymbol{\sigma}^D}{\sigma_{\text{vM}}^3}, \qquad \sigma_{\text{vM}} = \sqrt{\frac{3}{2}\boldsymbol{\sigma}^D : \boldsymbol{\sigma}^D}$$

  are not directly applicable to the damage variable.
- $\boldsymbol{D} \geq 0$ so that its invariants interpretation differs from the one for the stress tensor, which carries the loading sign.
- The damage state may be anisotropic, but its effect on elasticity close to be isotropic.

$\Rightarrow$ **the induced-damage anisotropy has also to be studied through the prism of elasticity, by the effective stiffness / compliance.**

Evolution of the norms during a tension test

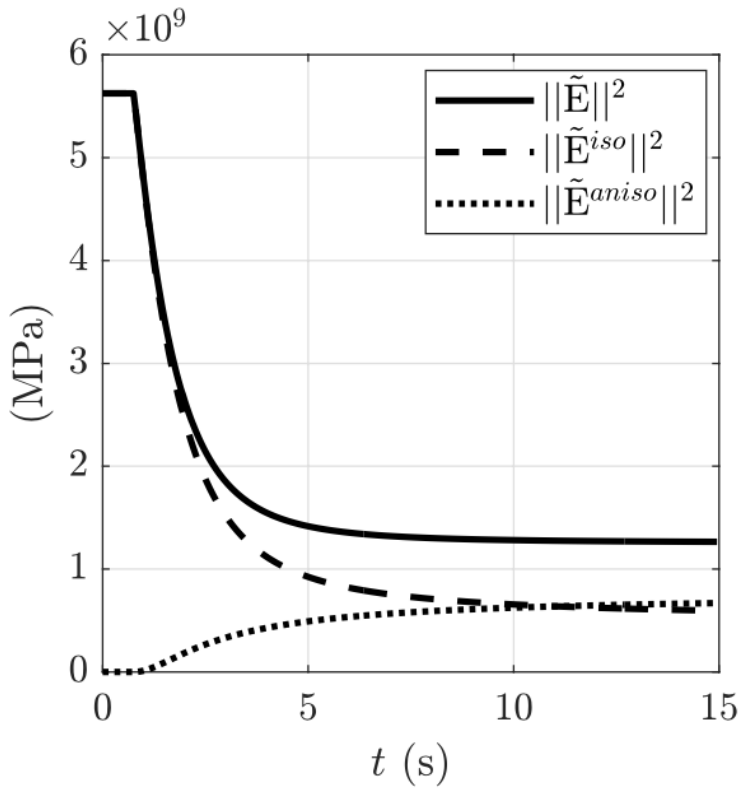

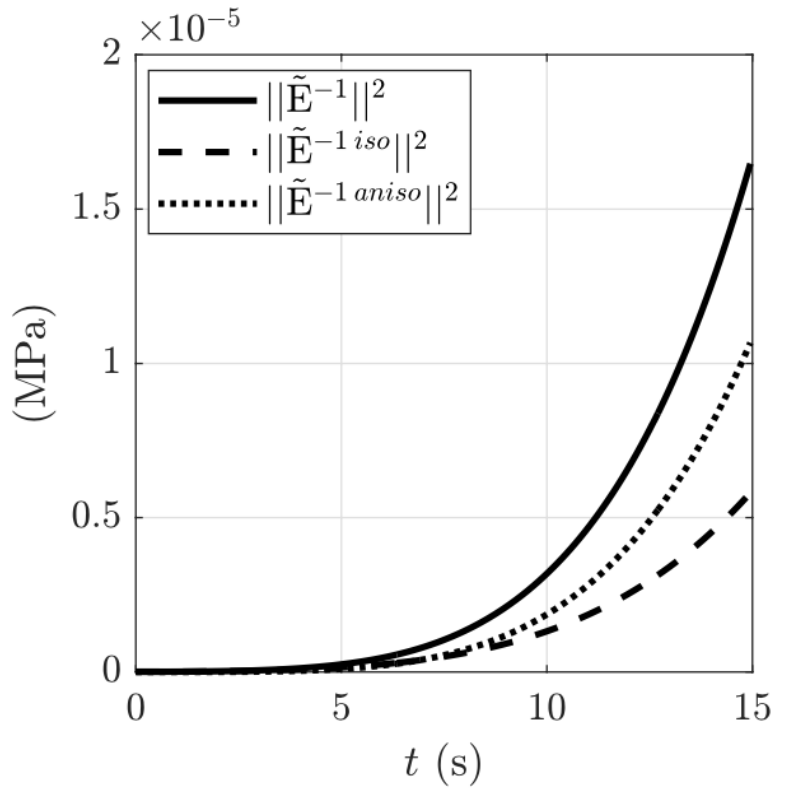

Relative distances to isotropy of $\tilde{\mathbb{E}}$, of $\tilde{\mathbb{S}}$

It appears pertinent to normalize the distances to isotropy.

1. to normalize them by the norm of the initial stiffness or compliance tensor, as

$$\frac{\Delta_{\tilde{\mathbb{E}}}}{\| \mathbb{E} \|} = \frac{\| \tilde{\mathbb{E}} - \tilde{\mathbb{E}}^{iso} \|}{\| \mathbb{E} \|} \quad \text{and} \quad \frac{\Delta_{\tilde{\mathbb{S}}}}{\| \mathbb{S} \|} = \frac{\| \tilde{\mathbb{S}} - \tilde{\mathbb{S}}^{iso} \|}{\| \mathbb{S} \|}.$$

2. to normalize the distance $\Delta_{\tilde{\mathbb{E}}}$ or $\Delta_{\tilde{\mathbb{S}}}$ by the norm of the isotropic part of the current effective stiffness or compliance tensors,

$$\delta_{\tilde{\mathbb{E}}} = \frac{\Delta_{\tilde{\mathbb{E}}}}{\| \tilde{\mathbb{E}}^{iso} \|} = \frac{\| \tilde{\mathbb{E}} - \tilde{\mathbb{E}}^{iso} \|}{\| \tilde{\mathbb{E}}^{iso} \|}, \quad \text{or} \quad \delta_{\tilde{\mathbb{S}}} = \frac{\Delta_{\tilde{\mathbb{S}}}}{\| \tilde{\mathbb{S}}^{iso} \|} = \frac{\| \tilde{\mathbb{S}} - \tilde{\mathbb{S}}^{iso} \|}{\| \tilde{\mathbb{S}}^{iso} \|}.$$

In the latter normalization, the references $\tilde{\mathbb{E}}^{iso}$ and $\tilde{\mathbb{S}}^{iso}$ evolve when damage grows.

Tension response

Computed macroscopic peak stresses close for all the concrete specimens

All specimens with same aggregate volume fraction

Higher discrepancy is exhibited in the post-peak stage.

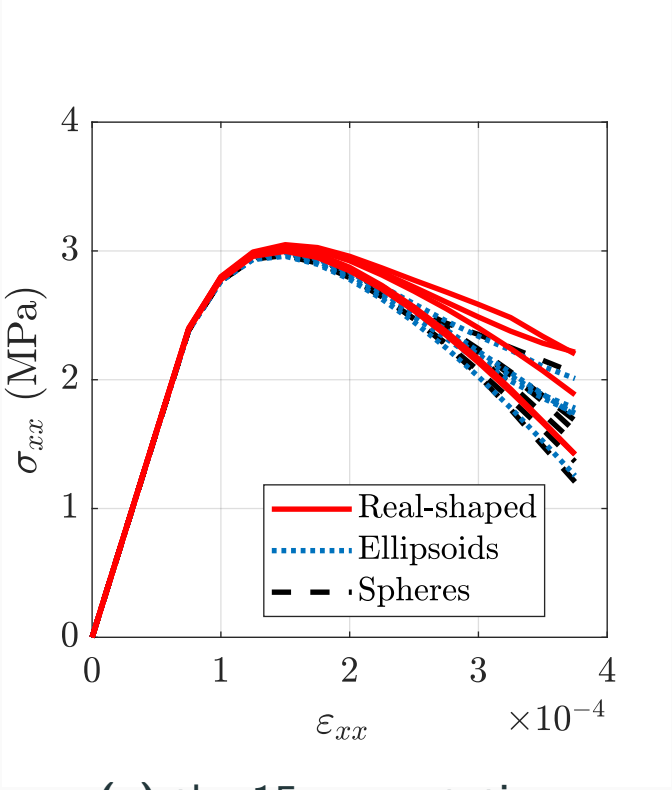

(a) the 15 computations

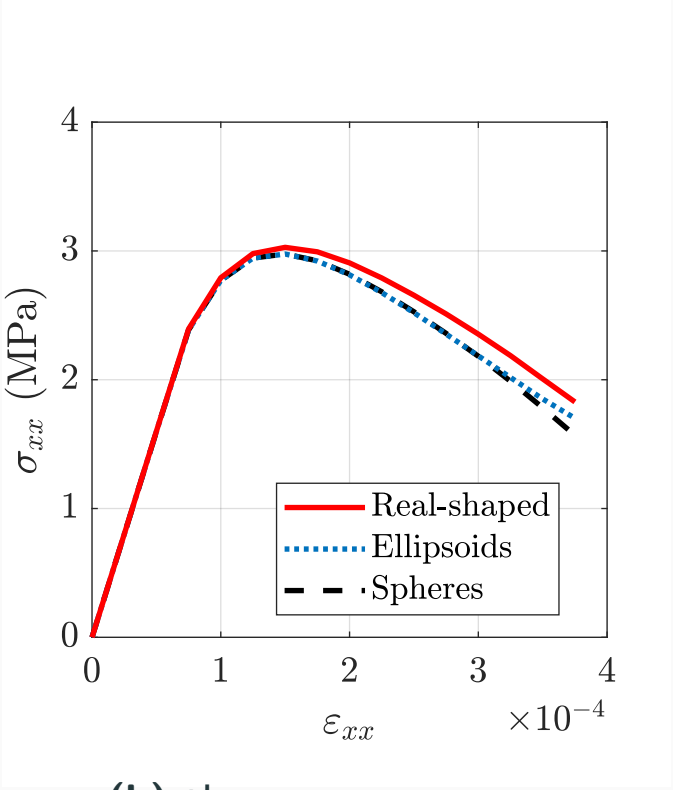

(b) the mean responses

Macroscopic stress-strain diagrams for tension

Monotonic responses

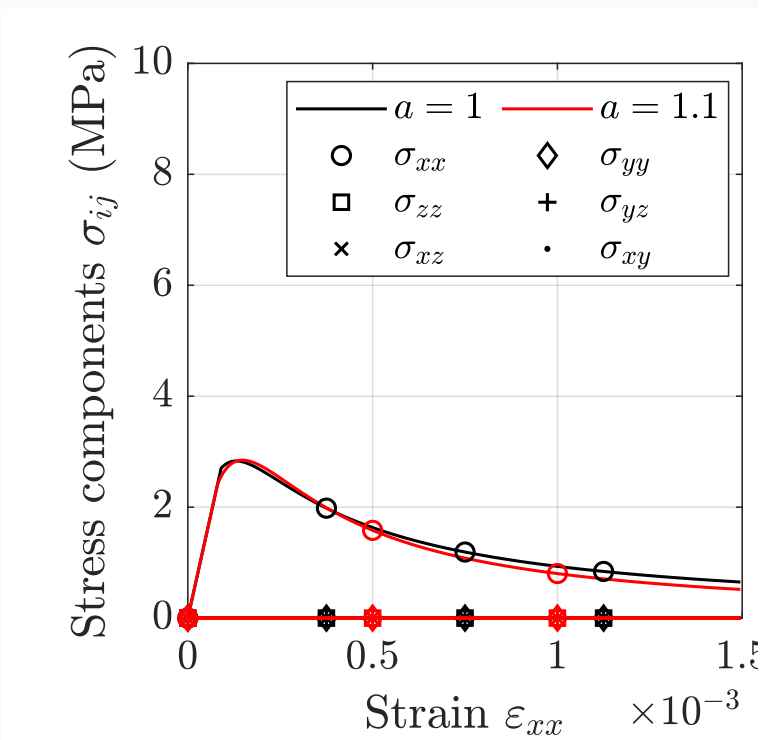

(a) Uniaxial tension

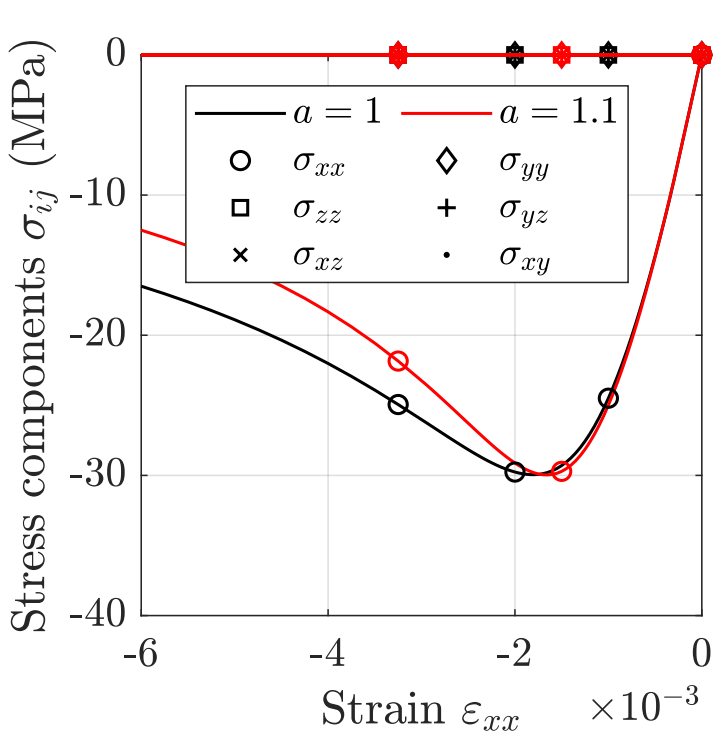

Uniaxial compression

Cyclic responses

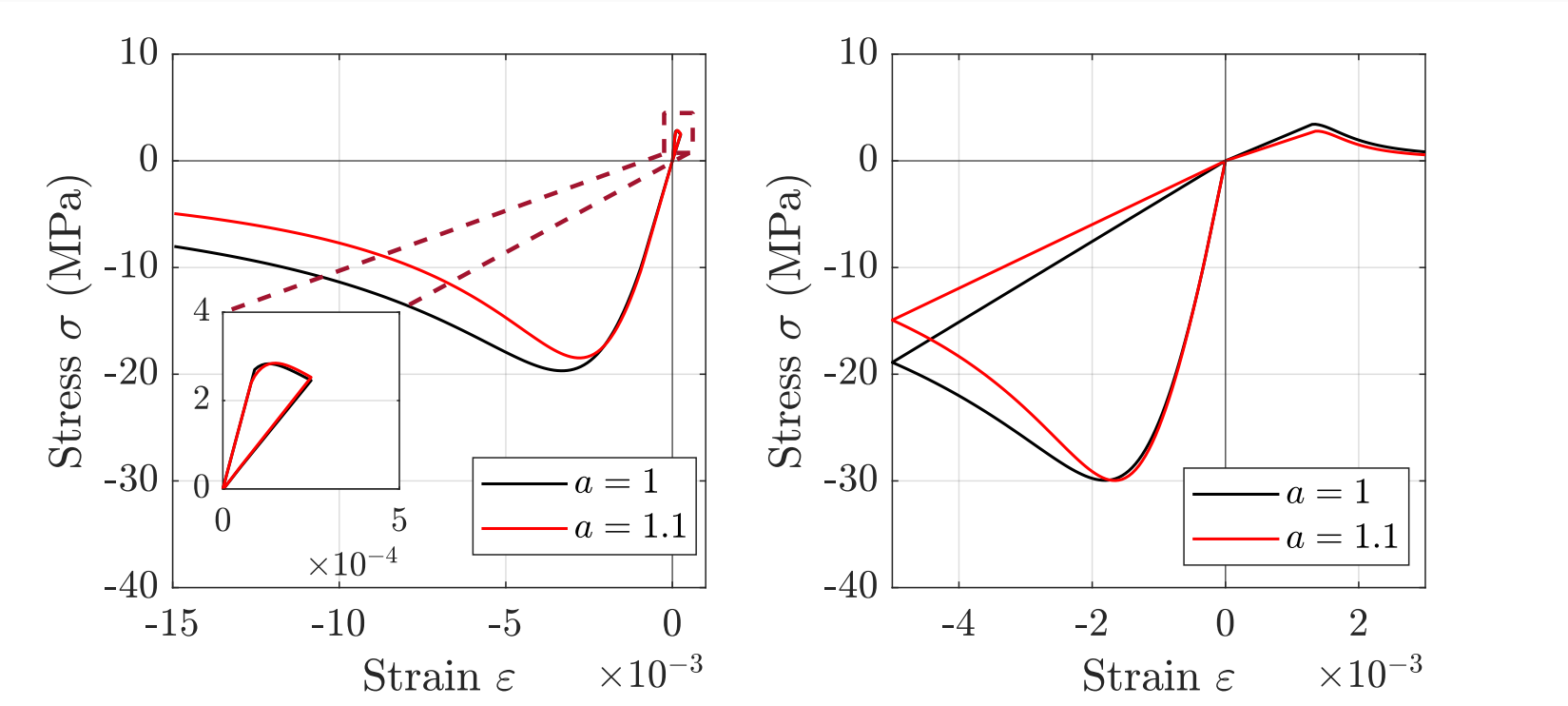

(a) Tension-Compression

(b) Compression-Tension

Virtual concrete response in monotonic tension

Coordinate-free indicators in case of tension loading

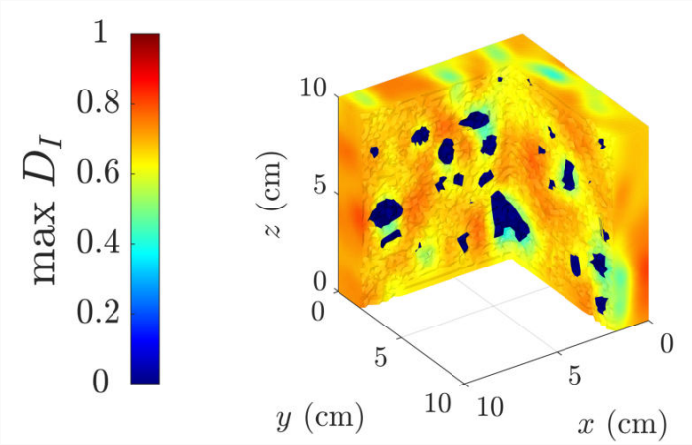

(a) max D_I for $U = 20$ μm.

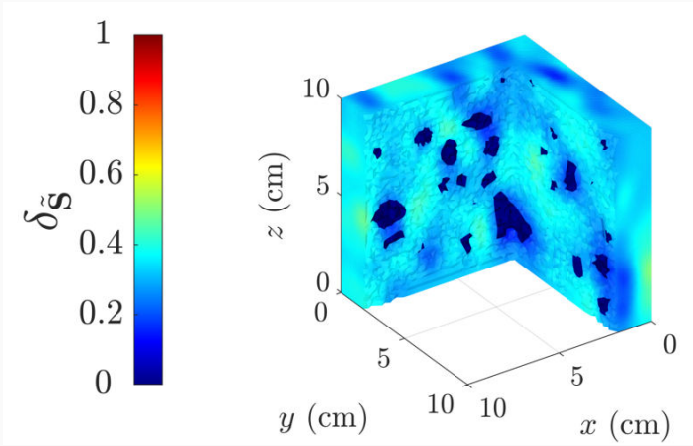

(b) Relative distance $\delta_{\tilde{\mathbb{S}}}$ for $U = 20$ μm.

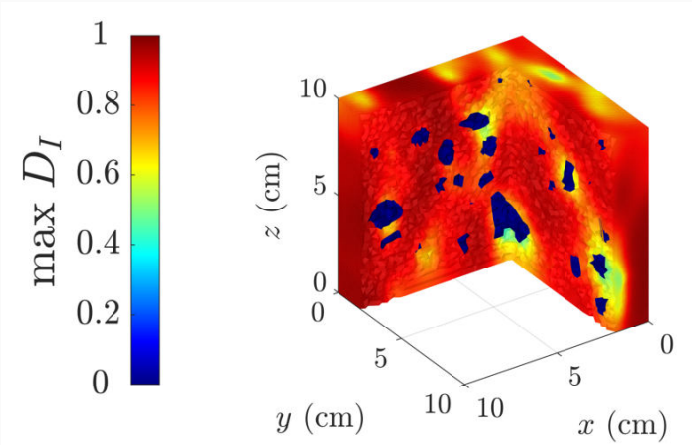

(c) max D_I for $U = 37.5$ μm.

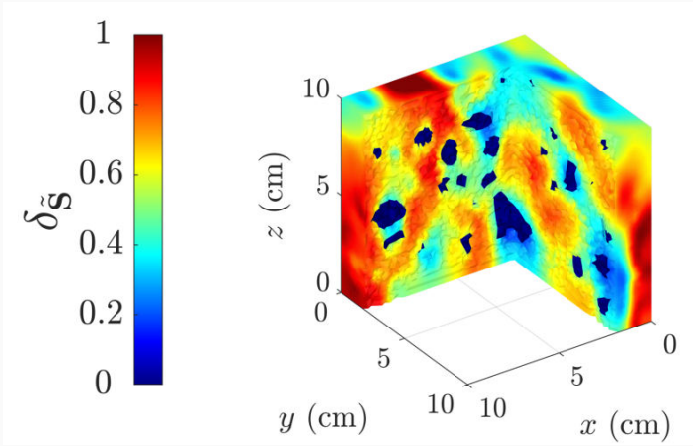

(d) Relative distance $\delta_{\tilde{\mathbb{S}}}$ for $U = 37.5$ μm.

Virtual concrete response in monotonic compression

Compression response

Computed macroscopic peak stresses rather close for all the concrete specimens (slightly higher for the laser-scanned aggregates)

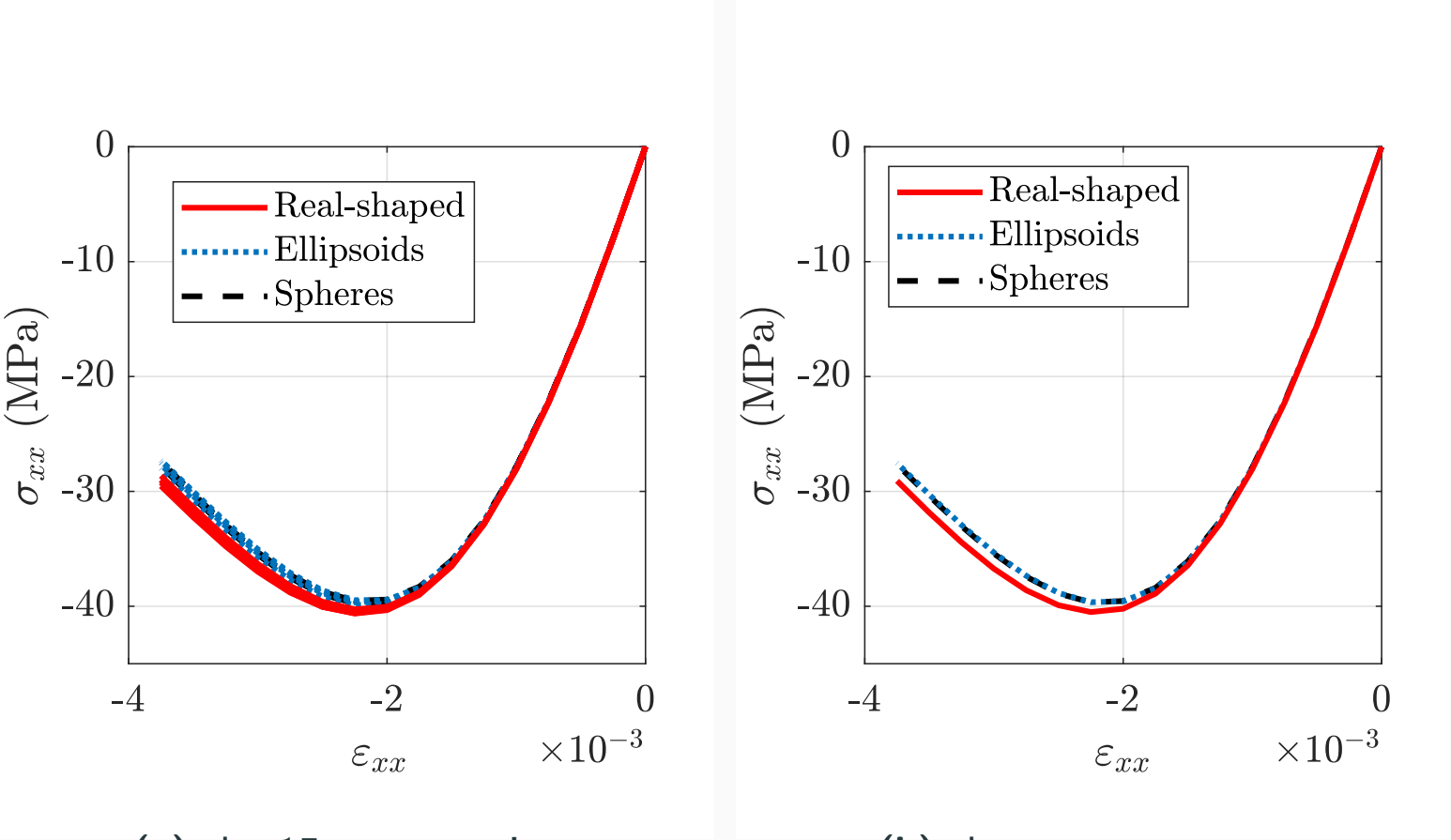

(a) the 15 computations **(b)** the mean responses

Macroscopic stress-strain diagrams for compression

Heterogeneous fields in compression

High levels of damage, more heterogeneous than in tension.

$\max D_I = D_1 \approx D_2$ almost identical to the second principal damage (damage state $\approx$ equibaxial).

Field of $\delta_{\tilde{\mathbb{S}}}$ more homogeneous over the mesostructure than in tension.

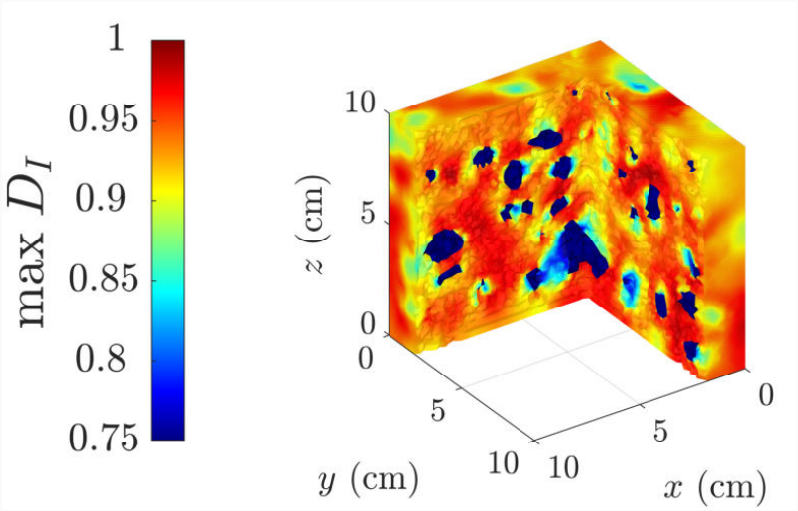

(a) $\max D_I$ **(b)** Relative distance $\delta_{\tilde{\mathbb{S}}}$.

At the end of computed post-peak in compression (at $U = 375$ μm)

Responses in cyclic loading

Concrete response in tension followed by compression

Five randomly packed specimens of each aggregate shape

Damaging tension (up to $U = 20\ \mu$m) followed by a compression loading.

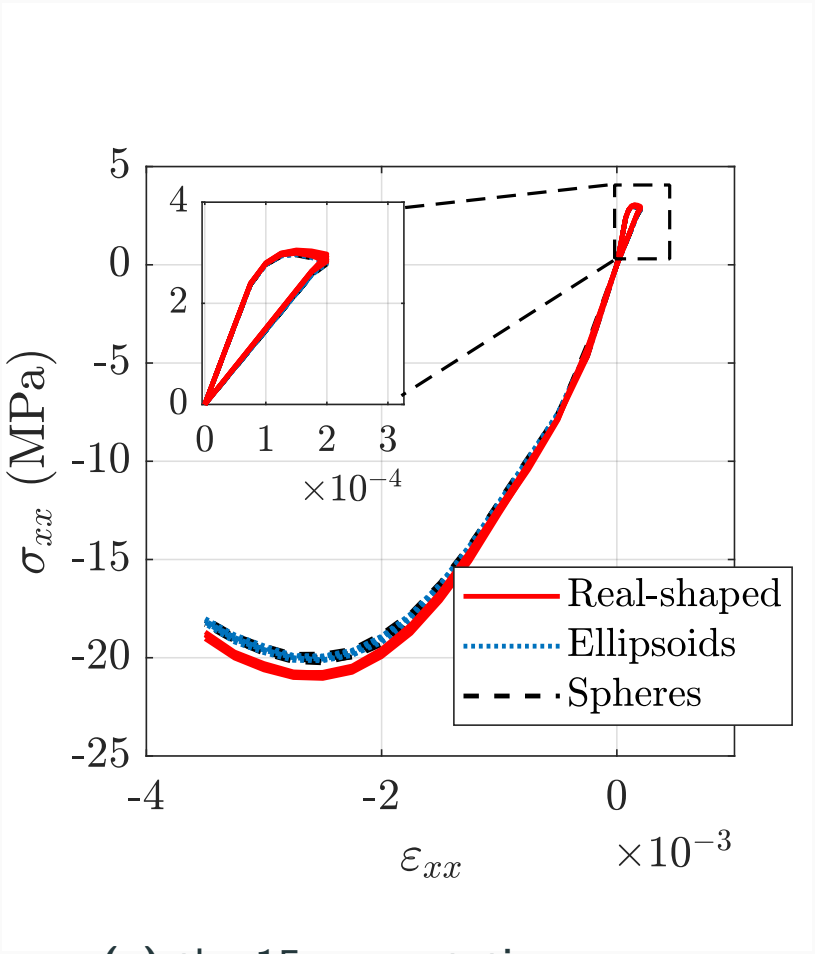

(a) the 15 computations

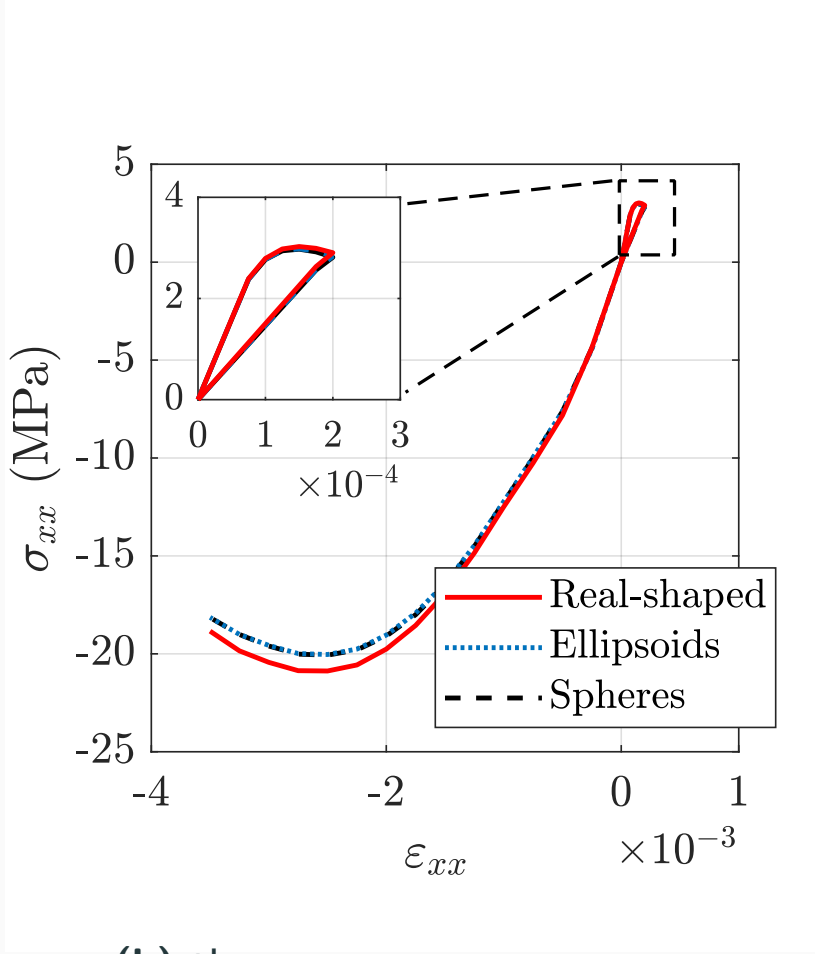

(b) the mean responses

Macroscopic stress-strain diagrams for an alternate tension-compression loading